UNITED STATES DEPARTMENT OF THE INTERIOR
GEOLOGICAL SURVEY

Earthquake Hazards in the Pacific Northwest of the United States

Compiled by
A. M. Rogers
T.J. Walsh
W.J. Kockelman
G.R. Priest

FOCAL MECHANISMS OF WESTERN WASHINGTON EARTHQUAKES AND THEIR RELATIONSHIP TO REGIONAL TECTONIC STRESS

BY LI MA[1], ROBERT CROSSON[1], AND RUTH LUDWIN[1]

Open-File Report 91-441-D

[1]University of Washington, Geophysics Program AK-50, Seattle, Wash. 98195

1991

Foreword

This paper is one of a series dealing with earthquake hazards of the Pacific Northwest, primarily in western Oregon and western Washington. This research represents the efforts of U.S. Geological Survey, university, and industry scientists in response to the Survey initiatives under the National Earthquake Hazards Reduction Program. Subject to Director's approval, these papers will appear collectively as U.S. Geological Survey Professional Paper 1560, tentatively titled "Assessing Earthquake Hazards and Reducing Risk in the Pacific Northwest." The U.S. Geological Survey Open-File series will serve as a preprint for the Professional Paper chapters that the editors and authors believe require early release. A single Open-File will also be published that includes only the abstracts of those papers not included in the pre-release. The papers to be included in the Professional Paper are:

Introduction

Rogers, A.M., Walsh, T.J., Kockelman, W.J., and Priest, G.R., "Earthquake hazards in the Pacific Northwest: An overview

Tectonic Setting

Paleoseismicity

Adams, John, "Great earthquakes recorded by turbidites off the Oregon-Washington margin"

Atwater, B.F., "Coastal evidence for great earthquakes in western Washington"

Nelson, A.R., and Personius, S. F., "The potential for great earthquakes in Oregon and Washington: An overview of recent coastal geologic studies and their bearing on segmentation of Holocene ruptures, central Cascadia subduction zone"

Peterson, C. D., and Darienzo, M. E., "Discrimination of climatic, oceanic, and tectonic forcing of marsh burial events from Alsea Bay, Oregon, U.S.A."

Tectonics/Geophysics

Goldfinger, C., Kulm, L.D., Yeats, R.S., Appelgate, B., MacKay, M., and Cochrane, G., "Active strike-slip faulting and folding in the Cascadia plate boundary and forearc, in central and northern Oregon"

Ma, Li, Crosson, R.S., and Ludwin, R.S., "Focal mechanisms of western Washington earthquakes and their relationship to regional tectonic stress"

Snavely, P. D., Jr., and Wells, R.E., "Cenozoic evolution of the continental margin of Oregon and Washington"

Weaver, C. S., and Shedlock, K. M., "Estimates of seismic source regions from considerations of the earthquake distribution and regional tectonics"

Yeats, R.S., Graven, E.P., Werner, K.S., Goldfinger, C., and Popowski, T.A., "Tectonic setting of the Willamette Valley, Oregon"

Earthquake Hazards

Ground Motion Prediction

Cohee, B.P., Sommerville, P.G., and Abrahamson, N.A., "Ground motions from simulated M_W=8 Cascadia earthquakes"

King, K.W., Carver, D.L., Williams, R.A., and Worley, D.M., "Site response studies in west and south Seattle, Washington"

Madin, I. P., "Earthquake-hazard geology maps of the Portland metropolitan area, Oregon"

Silva, W.J., Wong, I.G., and Darragh, R.B., "Engineering characterization of strong ground motions with applications to the Pacific Northwest"

Ground Failure

Chleborad, A. F., and Schuster, R. L., "Earthquake-induced ground failure associated with the April 13, 1949, and April 29, 1963, Puget Sound area, Washington, earthquakes"

Grant, W. P., Perkins, W. J., and Youd, L., "Liquefaction susceptibility maps for Seattle, Washington North and South Quadrangles

Earthquake Risk Assessment

Wang, Leon R.L., Wang, Joyce C.C., and Ishibashi, Isao, "GIS applications in seismic loss estimation model for Portland, Oregon water and sewer systems"

Implementation

Kockelman, W. J., "Techniques for reducing earthquake hazards--An introduction"

Booth, D.B., and Bethel, J.P., "Approaches for seismic hazard mitigation by local governments--An example from King County, Washington"

May, P.J., "Earthquake risk reduction prospects for the Puget Sound and Portland Areas"

Perkins, J.B., and Moy, K.K., "Liability for earthquake hazards or losses and its impacts on Washington's cities and counties"

Preuss, Jane, and Hebenstreit, G. T., "Integrated hazard assessment for a coastal community: Grays Harbor"

Contents

Illustrations

ABSTRACT

Tectonic stress in western Washington is investigated by inverting focal mechanisms for principal stress directions using the technique first presented by Gephart and Forsyth (1984). A total of 191 well constrained focal mechanisms were determined from data collected by the Washington Regional Seismograph Network. We examine differences between focal mechanisms of crustal and subcrustal earthquakes and also attempt to determine whether crustal stress in the Mt. St. Helens area, where focal mechanisms commonly have P axis azimuths in a NE direction, differs significantly from crustal stress in the Puget Sound region where mechanisms typically have P axis azimuths oriented NS.

For the comparison of crustal earthquakes (depth < 30 km) in the Puget Sound and Mt. St. Helens regions, the single best-fitting model for Puget Sound has a nearly NS σ_1 (maximum principal compressive stress) orientation with an EW σ_3 (minimum principal compressive stress) orientation, while the best-fitting model in the Mt. St. Helens area had NNE σ_1 orientation and ESE σ_3 orientation. At all confidence levels examined, the allowable stress orientations for these two regions overlap. From this analysis we conclude that there is no necessity to invoke reorientation of stress in the Mt. St. Helens region, although such reorientation is not precluded by the data. A uniform NS compressive tectonic stress in the crust is adequate to explain all of the observed focal mechanisms in western Washington.

In the subducted Juan de Fuca slab, the state of stress is more complex. Composites of P and T axes from focal mechanisms of subcrustal earthquakes (depths > 30 km) do not cluster around a single direction, although T axes are scattered about the general direction of plate subduction. Inversion for stress orientation indicates that no single set of stress directions adequately fits the observed focal mechanisms for subcrustal earthquakes within the subducted slab. The diversity of orientations of P and T axes of these intraslab earthquakes may be consistent with the hypothesis of an arched slab beneath Puget Sound which produces variations in the slab stress state.

The NS compressive tectonic stress in the continental crust and the dramatic change in stress state within the subducted Juan de Fuca slab indicate that the crustal stress is not controlled in a simple fashion by the processes causing plate convergence and subduction. We suggest that the magnitude of plate coupling stress may be significantly lower than the level of regional tectonic stress resulting from other causes.

INTRODUCTION

Only a limited number of geophysical methods provide insight into the state of tectonic stress. Direct stress measurements from borehole techniques reflect only near surface conditions, and have been utilized infrequently in the Pacific Northwest. Geodetic strain measurements provide information on changes and rates of change of stress indirectly through measurements of strain, and such measurements have been done only in limited numbers in the Pacific Northwest (Lisowski and others, 1987; Savage and Lisowski, 1991). Earthquakes reflect strain within the earth through slip on fault surfaces. This process is controlled by stress and the yield properties of the rock in question. By making reasonable assumptions about the relationships between stress and fault slip, we can infer the state of stress at midcrustal and greater depths through the study of earthquake focal mechanisms. With a relatively large number of earthquakes, statistical uncertainty in our knowledge of stress can be reduced. Midcrustal and subcrustal earthquakes are relatively abundant in western Washington, and the Washington Regional Seismograph Network (WRSN) places a powerful observational tool at our disposal for focal mechanism analysis. In this paper, we analyze focal mechanisms of western Washington earthquakes to establish the orientation of regional tectonic stress.

In the Pacific Northwest, we expect the tectonics to be strongly influenced by the subduction of the Juan de Fuca plate beneath the North American plate along the Cascadia subduction zone (CSZ) (e.g., Atwater, 1970; Riddihough, 1984). In subduction zones where strong coupling exists between the convergent plates, it is expected that the backarc should be characterized by tectonic compression normal to the arc (e.g., Uyeda and Kanamori, 1979). Since tectonic stress is the underlying physical mechanism driving earthquake hazards, it is of primary importance that we gain an understanding of regional tectonic stress in the Pacific Northwest. At shallow depths (less than 30-40 km) within subduction zones worldwide, it is common to observe (interplate) earthquakes that arise from direct slip between two plates. Stresses interpreted from these earthquakes are consistent with compression in the direction of plate convergence. At greater depths, earthquakes within the descending slab commonly reflect downdip tension or other stresses within the slab (e.g., Isacks and Molnar, 1971).

Interplate earthquakes have never been observed instrumentally along the CSZ, although active plate convergence is widely accepted. Previous focal mechanism studies indicate the general prevalence of NS compressive tectonic stress orientation based on earthquakes in both western and eastern Washington (Crosson, 1972; Yelin and Crosson, 1982; Malone and others, 1975; Crosson, 1983). This prevalence of NS compression is not easily interpreted in terms of our understanding of plate convergence in a N50°E direction (Riddihough, 1984), nor with the N70°E principal stress direction predicted from a simple mechanical model of plate interaction (Savage and others, 1981). Given strong plate coupling, we expect focal mechanisms of crustal earthquakes to reflect compression in the direction of convergence. The σ_1 orientation from focal mechanisms also disagrees with the principal compressive strain directions derived from geodetic observations as argued by Savage and others (1981), Lisowski and others (1987), and Savage and Lisowski (1991), although strain rates measured so far in the Pacific Northwest are generally of low magnitude compared to those in many other regions.

It may be possible to reconcile the earthquake and geodetic observations by noting that the geodetic measurements are sensitive to small changes in strain (and stress), whereas earthquakes should reflect the absolute ambient levels of stress in the crust (Sbar, 1982). Thus strain rate measurements may reflect small incremental changes in stress superimposed upon a much larger ambient tectonic stress field, and the two types of measurements need not agree in orientation. The implication of this argument is that the coupling stress due to subduction is small in magnitude relative to the background ambient tectonic stress due to other processes. Note that this does not necessarily mean that large subduction earthquakes can not be produced by this relatively low level of coupling stress, only that the stress driving subduction may be low in magnitude compared to regional ambient tectonic stress.

In the Mt. St. Helens region, focal mechanisms from earthquakes along the St. Helens seismic zone (Weaver and Smith, 1983) show rotation of P axes to the NE. This rotation was interpreted by Weaver and Smith to indicate a σ_1 driven more strongly by plate coupling in this region, suggesting a variation in plate coupling from north to south along the CSZ. In this paper, we further examine this important issue which bears directly on earthquake hazards.

The state of stress from intraslab earthquakes (i.e., earthquakes occurring within the subducting Juan de Fuca plate or "slab") has been far from clear. Since there is a known earthquake hazard in the Puget Sound region from subcrustal earthquakes, we may expect to gain insight into the origin and nature of this hazard through the study of intraslab focal mechanisms. Although past focal mechanism studies have suggested changes in orientation of stress from the subducted slab to the overlying North American plate, the extent of this difference has never been clearly quantified. Furthermore, although downdip extensional stress has been associated with slab earthquakes (Taber and Smith, 1985), not all intraslab mechanisms conform to this picture, as we will illustrate in this paper. Thus an objective of this paper is to clarify some of the uncertainties of interpretation of intraslab focal mechanisms and to ascertain if a coherent stress model can be interpreted for these earthquakes.

METHOD OF STRESS DETERMINATION

In conventional focal mechanism analysis, it is common to use the pattern of P and T axes as determined by individual focal mechanisms to infer the orientation of regional tectonic principal stress axes. A spatial scatter of axes may be averaged either qualitatively or quantitatively to establish "best" P and T axes. A possible difficulty with this approach became clear when McKenzie (1969) pointed out that if slip occurs on preexisting zones of weakness, there may be substantial deviation between the orientations of seismic P and T axes and the true principal axes of stress. In his paper, McKenzie established the theoretical basis for analyzing this problem. Since the earth's crust is commonly believed to have many fractures, faults, and zones of varying strength, the simplified interpretation of P and T axes may lead to erroneous conclusions regarding the true orientation of tectonic stress. A number of workers, among them Angelier (1979), subsequently developed quantitative methods of analyzing large amounts of geologic data, such as fault striations, to correctly estimate regional stress. Such methods are necessarily constrained to near surface conditions. Ellsworth and Zhonghuai (1980) extended these methods to the analysis of focal mechanisms.

Recently, Gephart and Forsyth (Gephart and Forsyth, 1984; Gephart, 1985, 1990a, 1990b) developed a complete and self-consistent method of inverting a group of focal mechanisms for the orientation of the regional tectonic stress tensor along with a quantitative indicator of the relative magnitudes of the principal stresses. This method is based on McKenzie's principle, and makes use of a scalar rotational misfit between the theoretical stress orientation that is currently being tested, and the stress orientation required to activate the observed fault planes. The sum of misfits is the objective function that is minimized to achieve a best fitting stress model, as well as to establish the statistical scatter of possible solutions. The actual slip plane for each earthquake may be assigned a priori or selected objectively by the processing algorithm. Gephart and Forsyth's method makes use of a "least rotation" principle to decide between the two possible slip planes established by each focal mechanism when the slip plane has not been a priori assigned. Formal statistical confidence limits are established for possible tectonic stress orientations that are

consistent with the observed focal mechanisms. For this method it is assumed that the magnitudes and directions of principal stresses do not change in a tectonic unit or over a region from which the earthquakes to be analyzed are selected. Therefore, it may be viewed as a test of the hypothesis that a single uniform regional stress explains the observed focal mechanisms.

SELECTION OF DATA

The WRSN comprises over 100 short period vertical component stations in Washington and northern Oregon (Qamar and others, 1987). Signals are telemetered to a central recording facility in real time and have been digitally recorded since 1980. Two horizontal component Wood-Anderson seismographs are also operated as part of the network. Although the network operated for about 10 years prior to 1980, only data acquired after that time are used for this study because of the quality improvement resulting from digital data acquisition. This improvement in quality is particularly important for focal mechanism studies, since the identification of P wave polarities, the main part of our data set, are usually clear from digital data but were often obscured on the older analog film records.

The following criteria were used to initially select earthquakes for focal mechanism analysis: (1) azimuthal gap of station coverage $\leq 100°$, (2) unweighted rms travel time residual ≤ 0.3 sec, (3) coda magnitude ≥ 1.0. Earthquake locations determined in normal preliminary processing were used for this study (e.g., Qamar and others, 1987). All events with 8 or more identified polarities were examined for possible inclusion in the data set; seismograms of promising events were reread for polarities and any known polarity reversals were corrected. Focal mechanisms were then constructed by hand fitting, and acceptable solutions retained for the inversion analysis. If a nodal plane could be rotated 20° or more, or the solution was deemed otherwise poorly constrained due to polarity discrepancies or other factors, the event was rejected. Since subcrustal earthquakes (within the subducted Juan de Fuca slab) are rarer than crustal events (Crosson, 1983), and relatively few focal mechanisms have been determined for this group, a special effort was made to include all possible subcrustal earthquakes. A total of 191 high quality focal mechanisms were ultimately retained for further analysis. These mechanisms and their associated polarity data are included in the Appendix. The data set is divided into three spatial groups consisting of: (a) shallow Puget Sound earthquakes, (b) deep Puget Sound earthquakes (subcrustal), and (c) shallow Mt. St. Helens region earthquakes. We individually analyzed all three groups, and discuss the significance of our results in light of regional stress orientation.

Figure 1 is an EW cross section plotting hypocenters of earthquakes used in this study. The Wadati-Benioff zone of subcrustal (deeper than 30 km) earthquakes is clearly separated from the shallower crustal earthquakes. Subcrustal seismicity is within the subducting slab, and not at the plate interface, and as noted earlier; we refer to these earthquakes as intraslab. The slab dip angle varies from 10°-12° in the Puget Sound area to 15°-20° north and south of Puget Sound (Green and others, 1986; Keach and others, 1986; Crosson and Owens, 1987).

FOCAL MECHANISMS

Crustal Earthquakes

Figure 2 is an epicenter map with the locations of all crustal earthquakes. The crustal focal mechanisms (hypocentral depths < 30 km) are divided into two groups. One group, 76 in number, includes earthquakes in the central Puget Sound region and western Cascades, and we refer to this group as "shallow Puget Sound". The second crustal group, with 73 earthquakes, lies in the Mt. St. Helens region which we refer to as "St. Helens".

We constructed focal mechanisms for a total of 149 crustal earthquakes in the combined Puget Sound and St. Helens groups. Of these, seventeen were larger than M 3.0 and are shown on Figure 3. Event numbers correspond to the Appendix listings, and all focal mechanism plots in this paper use lower hemisphere, equal area projections with black for compressional quadrants. Mechanisms for earthquakes located in the Puget Sound region have P axes varying generally from NNW to NNE and are of both thrust and strike-slip type. Only two of the events shown in Figure 3 are in the St. Helens group (events 48 and 140). Of these, event 48 has a mechanism similar to that of the 1981 Elk Lake mainshock (Grant and others, 1984). Both of the St. Helens events have strike-slip mechanisms that are typical of this region and less common in the Puget Sound region.

Figure 4 summarizes the shallow Puget Sound data set with a composite plot of P and T axes on a lower hemisphere equal area projection. From this figure, it can be seen that there is a strong preference for nearly NS P axes, with T axes more uniformly distributed in a girdle near the equator of the projection.

In the St. Helens region, 52 out of the 73 earthquakes were located along the northern part of the SHZ (Weaver and Smith, 1983) and 21 events scattered elsewhere in the region. In the subsequent analysis, we assumed that the slip planes of these 52 SHZ events were constrained to align approximately with the strike of the SHZ. Figure 5 is a composite plot of P and T axes for all of the St. Helens earthquakes. P axes tend to be oriented NE, suggesting apparent stress rotation either due to the existence of the St. Helens seismic zone itself, or due to larger regional tectonic variations.

Subcrustal Earthquakes

Figure 6 is an epicenter map of the 42 subcrustal or deep Puget Sound earthquakes. Most are located on the western side of Puget Sound and beneath the eastern side of Olympic Peninsula. Focal mechanisms for subcrustal earthquakes are shown in Figure 7. In Figure 7, events 3 and 116 are larger than magnitude 4.0 and the remaining events are between magnitude 3.0 and magnitude 4.0. Both 3 and 116 have vertical P axes and nearly horizontal T axes, but one T axis is oriented north and the other oriented southeast. These two normal events suggest an extensional environment beneath the convergent margin, in agreement with Taber and Smith (1985). However, the two events have very different apparent stress orientations. Event 3, located in the northeast corner of the Olympic Peninsula at a depth of 48.5 km, has a nearly NS T axis. On the other hand, event 116, at the south end of the Olympic Peninsula, has a SE T axis. A careful examination of the mechanisms shown in Figure 7 reveals the lack of obvious consistency among mechanisms in this group. It is difficult to generalize about the state of stress within the subducted slab except to say that there may be a prevalence of horizontal T axes.

As another way to view this variability, plots of P and T axes for all subcrustal earthquakes are shown on lower hemisphere equal area stereonet plots in Figure 8. P axes vary in plunge from near vertical to near horizontal with azimuths varying from northeast to southeast and from northwest to southwest. Since we do not observe P axes near NS as we do with the crustal suite of earthquakes, we conclude qualitatively that these data are not consistent with the NS compression noted earlier for crustal earthquakes, and that there is a major change in stress state from the subducted Juan de Fuca slab to the overlying North American plate.

STRESS ANALYSIS

We applied the inversion technique of Gephart and Forsyth (1984) to the three groups of focal mechanisms in western Washington. The output of the inversion calculations includes the best fitting principal stress axis orientations (for σ_1, σ_2, and σ_3), the distribution of acceptable orientations for each axis at the specified confidence level, and the best fitting R value where R is defined as

$$R = \frac{(\sigma_1 - \sigma_2)}{(\sigma_1 - \sigma_3)}.$$

Thus R is a measure of whether the intermediate principal stress is near the maximum ($R \sim 0$) or near the minimum ($R \sim 1$) principal stress. In addition, the mean value of misfit for the best fitting values is given as an angular rotation (Gephart and Forsyth, 1984). The inversion calculations involve a modified grid search method where we may predefine the allowable ranges of search for efficiency.

Shallow Puget Sound Earthquakes

For this data set, since there is a general consistency based on the P and T axis distribution, we limited the grid search values for σ_1 used in the inversion. The ranges in azimuth selected were from N60°W to N60°E and from S57°E to S63°E. The allowed range of plunge was set from 1° to 51°. An angular increment between grid points of 5° was used for both azimuth and plunge. The result of setting these parameters is that 11,000 discrete stress orientations are tested for each R value where R varies between .1 and 1.0 in steps of 0.1.

For the shallow Puget Sound data set, the best fitting model (also summarized in Table 1) is (azimuth, plunge): σ_1 = (356°, 1°), σ_2 = (262°, 72°), and σ_3 = (86°, 18°). The value of R yielding the best fit is 0.6. Figure 9 shows the allowable σ_1 orientations at both 50% and 95% confidence levels. Note that the 50% confidence limit provides a better feel for the orientation of the best fit solution. In agreement with our intuition based on the distribution of P and T axes, we see that the best fitting σ_1 is nearly horizontal and oriented NS. For the best fitting stress axis model, the 76 earthquakes have an average misfit of 12.6°, and all but 15 have misfits of less than 20°, suggesting that the single NS compression model is a good representation of the regional stress. This result supports and refines previous findings for the region (Crosson, 1972; Sbar, 1982; Rogers, 1979; Malone and others, 1975; Yelin and

Crosson, 1982; Yelin, 1982; Crosson and Frank, 1975; Crosson and Lin, 1975). To test the stability of the inversion to outlier data, the computations were repeated after individually removing focal mechanisms with misfits greater than 20°. The results were virtually unchanged, suggesting that our data set is large enough to produce stable and robust results.

TABLE 1 - STRESS INVERSION RESULTS

Region	No. of events	σ_1		σ_2		σ_3		R	misfit
		az.	pl.	az.	pl.	az.	pl.		
Shallow Puget Sound	76	356°	1°	262°	72°	86°	18°	0.6	12.6°
Mt. St. Helens Area	73	203°	1°	106°	81°	293°	9°	0.7	9.1°
Subcrustal Puget Sound	42	245°	51°	13°	26°	117°	26°	0.1	19.9°

Mt. St. Helens Earthquakes

A total of 73 mechanisms were inverted for the St. Helens region data set. We used the same orientation grid constraints as described for the Puget Sound region, and the same increments for R. Although the inversion technique will normally select the appropriate slip plane using a minimum rotation criterion, when external knowledge of the slip plane is available it can (and should) be specified a priori. The existence of a linear zone of epicenters over 50 km long extending from Mt. St. Helens to the NNW allowed us to select the slip plane in 59 of the events analyzed under the assumption that this is a strike-slip crustal fault zone. For this group, nodal planes with strikes within 15° of NS were judged to be aligned along the St. Helens seismic zone and were selected as fault planes.

The single best-fitting model found for all 73 Mt. St. Helens focal mechanisms is: σ_1 = (203°, 1°), σ_2 = (106°, 81°), σ_3 = (293°, 9°) with R = 0.7. Figure 10 shows the allowable σ_1 axis orientations at the 50%, and 95% confidence levels. The average misfit for all events in this example is 9.1° and 9 events have misfit greater than 20°. We note here that at both 95% and 50% confidence levels, the allowable P axis orientations for the St. Helens region overlap those for the shallow Puget Sound distribution.

Subducted Slab Earthquakes

If we assume that uniform stress causing slip on preexisting faults can be equally applied to earthquakes at subcrustal depths, then we can apply the inversion method to investigate the stress state in the subducted Juan de Fuca slab. Composite plots of P and T axes from focal mechanisms of subcrustal earthquakes in Puget Sound (Figure 4) do not show a clustered distribution of P and T axes, and so for this case it was necessary to use a stress grid with σ_1 directions covering the entire focal sphere.

Figure 11 shows the inversion result from the subcrustal deep Puget Sound focal mechanisms. The best-fitting model is: σ_1 = (245°, 51°); σ_2 = (13°, 26°); σ_3 = (117°, 26°) with R = 0.1. This low value of R means that the intermediate and maximum principal stress are close in magnitude, with the minimum principal stress significantly smaller than the other two. This result is in general agreement with the the expected extensional stress state along the top surface of a bending slab (Isacks and Molnar, 1971). Furthermore, the scatter of allowable solutions at the 50% and 95% confidence levels indicates that the single stress orientation model is not a satisfactory explanation for the range of focal mechanisms observed. We suggest that the slab is in a heterogeneous stress state perhaps resulting from the complications in slab geometry noted by Crosson and Owens (1987) (see also, Weaver and Baker, 1988). It is certain from these results, however, that the state of stress in the subducted slab is significantly more complex and differs from the state of stress in the continental crust of the North American plate.

DISCUSSION AND CONCLUSIONS

The results of this study confirm and extend the general NS horizontal tectonic compression in the North American plate of Washington first suggested by Crosson (1972). Although the best-fitting model found in the Mt. St. Helens area has σ_1 rotated about 27° to the NE relative to the Puget Sound region, the overlap of preferred stress

models at the 95% confidence level suggests that there is no requirement for a rotation of tectonic stress between these two regions. However, such a rotation is also not precluded by the data.

Our results offer an alternative explanation to the suggestion by Weaver and Smith (1983) that the rotation of stress indicates a change in stress coupling along the subduction zone. We prefer, in the absence of evidence to the contrary, to believe that a more uniform NS regional tectonic compressive stress is dominant and best explains the focal mechanism data with the fewest complicating assumptions. The apparent rotation at St. Helens is likely to be an artifact resulting from preferred slip on the pre-existing St. Helens zone of crustal weakness. We note that NS compression is the dominant tectonic characteristic along the west coast of United States (Zoback and Zoback, 1980; Sbar, 1982). Because of the rather limited extent of the Juan de Fuca plate in relationship to the extensive San Andreas and Queen Charlotte right lateral transform fault systems which form most of the remainder of the western plate boundary of North America, it appears that the stress state of the North American plate in western Washington is influenced mainly by the large scale transform motion between the Pacific and North American plates (Zoback and Zoback, 1980).

The accumulation of tectonic strain observed by geodetic measurements (Savage and others, 1981; Lisowski and others, 1987; Savage and Lisowski, 1991) appears to be in conflict with the NS compression interpreted from the focal mechanism analysis. It is important to note, however, that the geodetically observed strain rate is very low ($< 0.10\ \mu$ strain/yr) (Lisowski and others, 1987; Savage and Lisowski, 1991) and that strain measurements reflect only incremental changes in stress whereas focal mechanisms probably reflect the regional ambient stress. Furthermore, it is possible that the geodetic measurements may reflect inelastic deformation, in which case the principal strain axes need not reflect the deep state of stress. If the explanation lies with the magnitude of ambient and incremental stress, then clearly the plate coupling stress giving rise to the observed strain must be much smaller in magnitude than the ambient tectonic stress that causes most intraplate earthquakes.

The stress state in the slab appears to be complicated, and is not well described by a single stress model. The initial assumption of Gephart and Forsyth's method, that slip occurs on pre-existing planes of weakness, may not apply to the slab. However, the wide scatter of P and T axes directions suggests an inhomogeneous stress field. Viewing the composite plots of P and T axes, (Figure 8), it is difficult to even estimate directions of apparent compression and tension. There are, however, two clear characteristics: first, there are no P axes with NS azimuths and shallow plunge angles; secondly, the T axes are generally oriented northeast or southeast with shallow plunge angles. The difference between subcrustal P and T axes (Figure 8) and those of crustal earthquakes (Figures 4 and 5) indicates that there is little direct stress coupling between the crust and the deeper part of the subducted slab. Rather, the slab stress distribution appears to be generated largely by processes internal to the slab itself (e.g., bending stresses). At this point, we don't fully understand the implication of these results for intraslab earthquake hazards. However, a more complete understanding of both the slab structure and its stress state may allow us to place realistic bounds on the source parameters of future slab earthquakes. Although the spatial coincidence of the crustal and subcrustal earthquake suites in the Puget Sound region is not perfect (Figure 1), it is nevertheless puzzling in view of the difference in stress states, that these two zones of earthquakes do occur in general spatial proximity.

The variety of the directions of tensional axes in different parts of the slab might be due to superposition of down-dip tension on compressional stresses due to the plate arch. To test this possibility, we attempted to examine the slab stress axis orientations in light of the best available knowledge of slab geometry. Figure 12 is a north-south cross section with slab T axes projected onto the plane of the cross section. The shape of the slab at several longitudes is indicated by contours adapted from the model of Crosson and Owens (1987). From this plot, there appears to be a preference for T axes to lie in the plane of the arch or in a down-dip direction. For higher magnitude events this tendency may be even more pronounced. For example, five of the eight earthquakes with magnitudes equal to or greater than 3.0 had T axes along the arched slab, one had a T axis in the down-dip direction, and two had T axes at angles to the slab. These results suggest that the arching of the slab could result in the tension due to "hoop" stress or bending stress in the slab. The superposition of gravitational forces would further complicate this picture. The configuration of P axes, shown in Figure 13, is quite different. In this case, there appears to be a tendency for P axes to be normal to the slab surface.

In conclusion, we have found that the western part of the North American plate is likely to be in a state of uniform regional NS compressive tectonic stress that does not directly reflect the active subduction along the Cascadia subduction zone. Plate coupling stress appears to be of much lower magnitude than the regional NS compressive stress. There is no need, based on focal mechanism data, to invoke a rotation of stress in the vicinity of Mt. St. Helens, although such a rotation is not excluded by the data. The state of stress in the subducted Juan de Fuca plate is distinctly different and more complex than that in the overlying North American plate. The lack of a uniform stress state in the subducted slab indicates that plate geometry variations may play an important part in controlling slab stress and seismicity. In view of the apparent stress decoupling of crustal and subcrustal earthquakes in the Puget Sound region, the spatial coincidence of these two zones remains enigmatic.

ACKNOWLEDGMENTS

We thank Dr. John Gephart for providing the original programs to do this analysis, and for assistance in their use. This study is supported by the U.S. Geological Survey under Grant 14-08-0001-G1080 and 14-08-0001-G1390.

REFERENCES CITED

Angelier, J., 1979, Determination of the mean principal directions of stresses for a given fault population: Tectonophysics, v. 56, p. T17-T26.

Atwater, T., 1970, Implications of plate tectonics for the Cenozoic tectonic evolution of western North America: Geological Society of America Bulletin, v. 81, p. 3513-3536.

Crosson, R.S., 1972, Small earthquakes, stucture, and tectonics of the Puget Sound region: Bulletin of the Seismological Society of America, v. 62, p. 1133-1171.

1983, Review of seismicity in the Puget Sound region from 1970 through 1978: Proceedings of Workshop XIV, Earthquake Hazards of the Puget Sound Region, Washington, USGS Open File Report, 83-19, J.C. Yount and R.S. Crosson, Editors, U.S. Geological Survey, p. 6-18.

Crosson, R.S. and D. Frank, 1975, The Mt. Rainier earthquake of July 18, 1973 and its tectonic significance: Bulletin of the Seismological Society of America, v. 65, p. 393-401.

Crosson, R.S. and J.W. Lin , 1975, A note on the Mt. Rainier earthquake of April 20, 1974: Bulletin of the Seismological Society of America, v. 65, p. 549-556.

Crosson, R.S. and T.J. Owens, 1987, Slab geometry of the Cascadia subduction zone beneath Washington from earthquake hypocenters and teleseismic converted waves: Geophysical Research Letters, v. 14, p. 824-827.

Ellsworth, W.L. and X. Zhonghuai, 1980, Determination of the stress tensor from focal mechanism data (Abstract): EOS, Transactions of the American Geophysical Union, v. 61, p. 1117.

Gephart, J.W. and D.W. Forsyth, 1984, An improved method for determining the regional stress tensor using earthquake focal mechanism data - Application to the San Fernando earthquake sequence: Journal of Geophysical Research, v. 89, p. 9305-9320.

Gephart, J.W., 1985, Principal stress directions and the ambiguity in fault plane identification from focal mechanisms: Bulletin of the Seismological Society of America, v. 75, no. 2, p. 621-625.

1990a, FMSI: a FORTRAN program for inverting fault/slickenside and earthquake focal mechanism data to obtain the regional stress tensor: Computers and Geosciences, v. 16., no. 7, p. 953-989.

1990b, Stress and the direction of slip on fault planes: Tectonics, v. 9, no. 4, p. 845-858.

Grant, W.C., C.S. Weaver, and J.E. Zollweg, 1984, The 14 February 1981 Elk Lake, Washington earthquake sequence: Bulletin of the Seismological Society of America, v. 74, p. 1289-1309.

Green, A.G., R.M. Clowes, C.J. Yorath, C. Spencer, E.R. Kanasewich, M.T. Brandon, and A.S. Brown, 1986, Seismic reflection imaging of the subducting Juan de Fuca plate: Nature, v. 319, p. 210-213.

Isacks, B. and P. Molnar, 1971, Distribution of stresses in the descending lithosphere from a global survey of focal-mechanism solutions of mantle earthquakes: Reviews in Geophysics and Space Physics, v. 9, p. 103-174.

Keach, R.W., C.J. Potter, J.E. Oliver, and L.D. Brown, 1986, Cenozoic active margin and shallow Cascades structure: COCORP results from western Oregon (Abstract), Geological Society of America Abstracts with Programs, v. 18, p. 652, San Antonio.

Lisowski, M., J.C. Savage, and W.H. Prescott, 1987, Strain accumulation along the Cascadia subduction zone in Western Washington (Abstract): EOS, Transactions of the American Geophysical Union, v. 68, p. 1240.

Malone, S.D., G.H. Rothe, and S.W. Smith, 1975, Details of microearthquake swarms in the Columbia Basin, Washington: Bulletin of the Seismological Society of America, v. 65, p. 855-864.

McKenzie, D.P., 1969, The relation between fault plane solutions for earthquakes and the directions of the principle stresses: Bulletin of the Seismological Society of America, v. 59, p. 591-601.

Qamar, A., R. Ludwin, R.S. Crosson, and S.D. Malone, 1987, Earthquake hypocenters in Washington and northern Oregon - 1982-1986: Washington Department of Natural Resources, Division of Geology and Earth Resources: Information Circular 84, 78 p.

Riddihough, R.P., 1984, Recent movements of the Juan de Fuca plate system: Journal of Geophysical Research, v. 89, p. 6980-6994.

Rogers, G.C., 1979, Earthquake fault plane solutions near Vancouver Island: Canadian Journal of Earth Sciences, v. 16, p. 523-531.

Savage, J.C., M. Lisowski, and W.H. Prescott, 1981, Geodetic strain measurements in Washington: Journal of Geophysical Research, v. 86, p. 4929-4940.

Savage, J.C. and M. Lisowski, 1991, Strain measurements and the potential for a great subduction earthquake off the coast of Washington: Science, v. 252, p. 101-103.
Sbar, M.L., 1982, Delineation and interpretation of seismotectonic domains in western North America: Journal of Geophysical Research, v. 87, p. 3919-3928.
Taber, J.J. and S.W. Smith, 1985, Seismicity and focal mechanisms associated with the subduction of the Juan de Fuca plate beneath the Olympic Peninsula, Washington: Bulletin of the Seismological Society of America, v. 75, p. 237-249.
Uyeda, S. and H. Kanamori, 1979, Back-arc opening and the mode of subduction: Journal of Geophysical Research, v. 84, p. 1049-1061.
Weaver, C.S. and S.W. Smith, 1983, Regional tectonic and earthquake hazard implications of a crustal fault zone in southwestern Washington: Journal of Geophysical Research, v. 88, 10,371-10,383.
Weaver, C.S. and G.E. Baker, 1988, Geometry of the Juan de Fuca place beneath Washington and northern Oregon from seismicity: Bulletin of the Seismological Society of America, v. 78, p. 264-275.
Yelin, T.S. and R.S. Crosson, 1982, A note on the south Puget Sound basin magnitude 4.6 earthquake of 11 March 1978 and its aftershocks: Bulletin of the Seismological Society of America, v. 72, p. 1033-1038.
Yelin, T.S., 1982, The Seattle earthquake swarms and Puget Basin focal mechanisms and their tectonic implications: M.S. Thesis, Geophysics Program, University of Washington, Seattle, WA.
Zoback, M.L. and M. Zoback, 1980, State of stress in the conterminous United States: Journal of Geophysical Research, v. 85, p. 6113-6156.

APPENDIX: FOCAL MECHANISM LISTINGS AND PLOTS

EXPLANATION

This appendix lists all focal mechanisms used in this study. All mechanisms were constructed by hand from polarity data reread from the original digital seismograms. The focal sphere plots are all lower hemisphere, equal area stereonet projections. Closed symbols represent compression, and open symbols represent dilatation for vertical component P wave arrivals. The strength of first motion is indicated as follows; strong compression is shown as an asterisk, less strong compression as an "X", weaker compression as a smaller asterisk, and weakest as a small "x"; strong dilatation is shown as an octagon, less strong as a triangle, weaker dilitation is shown as a small octagon, and weakest as a small triangle. Corrections have been made for stations known to have been reversed. Takeoff angles at the focal sphere were computed using a local velocity model with a linear increase in velocity with depth, approximating the regional velocity model used for the earthquake locations. This procedure smooths out the discontinuous jumps in takeoff angle introduced by the direct use of the discrete layered model for takeoff angle calculations. A small square is placed in the center of any symbol whose ray leaves the source at an upgoing angle. The tables and plots are separated into the three regions analyzed in the paper. The event numbers (#) are sequential in time.

TABLE A.1 - SHALLOW PUGET SOUND EARTHQUAKES

#	Date	Lat	Lon	Depth	Mag	P-axis		T-axis		Plane A		Plane B	
						az.	pl.	az.	pl.	az.	pl.	az.	pl.
14	820102	47.37	122.39	14.47	2.7	162	4	72	6	207	83	117	89
17	820123	46.61	121.43	3.33	3.2	180	45	90	0	215	60	325	60
26	820303	45.99	122.44	11.78	2.1	30	0	120	0	345	90	75	90
29	820310	46.74	122.20	16.71	2.4	192	4	285	38	322	61	65	67
30	820310	47.33	122.71	26.79	2.9	16	0	106	0	331	90	61	90
38	820404	46.57	122.48	19.53	1.9	182	38	89	4	218	61	322	68
41	820414	47.71	122.52	27.28	3.4	6	8	101	33	138	61	238	73
55	820718	46.58	121.39	6.48	2.9	5	0	95	0	320	90	50	90
58	820926	46.87	121.12	3.25	3.4	192	20	285	8	330	70	237	82
61	821015	47.59	122.63	27.52	3.0	38	18	284	51	89	40	334	71
63	821112	47.69	122.69	24.54	2.8	6	0	96	30	137	69	235	69
67	821211	47.53	122.73	20.22	2.3	5	17	101	18	143	65	233	89
70	821218	47.89	122.53	23.17	2.8	10	5	190	85	100	40	280	50
71	821220	46.59	121.42	5.26	2.7	15	37	108	4	158	61	56	68
72	821231	47.19	122.08	14.27	2.4	26	36	132	21	175	48	76	81
73	830124	47.11	121.99	6.62	3.0	342	15	162	75	72	30	252	60
75	830131	46.67	122.33	17.91	2.2	358	0	88	66	110	50	246	50
78	830303	47.64	121.94	2.35	2.9	346	0	76	0	301	90	31	90
80	830313	46.24	122.69	15.40	2.9	18	0	108	0	333	90	63	90
81	830315	46.52	122.79	24.05	2.7	36	46	127	0	182	59	71	60
84	830407	46.63	122.42	16.07	1.9	20	0	110	0	335	90	65	90
85	830409	46.74	121.82	8.27	1.8	170	7	272	60	289	46	56	58
90	830424	46.54	121.45	4.97	2.7	354	0	84	0	309	90	39	90
92	830504	48.34	122.10	8.68	2.9	2	30	266	10	40	61	137	77
94	830516	47.49	122.58	24.17	2.0	335	67	65	0	134	49	356	49
95	830519	47.64	122.50	23.48	2.0	28	0	118	62	143	51	273	51
97	830521	47.36	121.49	11.69	2.8	163	11	256	14	299	72	30	88

TABLE A.1 - SHALLOW PUGET SOUND EARTHQUAKES (CONT.)

#	Date	Lat	Lon	Depth	Mag	P-axis		T-axis		Plane A		Plane B	
						az.	pl.	az.	pl.	az.	pl.	az.	pl.
99	830525	47.78	121.71	10.72	3.0	180	16	275	16	317	67	231	90
100	830605	46.54	122.73	23.73	2.3	198	36	291	4	341	62	239	69
102	830726	46.69	122.54	17.35	2.2	199	3	98	75	274	44	123	50
103	830728	46.06	122.81	16.06	2.4	20	0	110	57	139	54	261	54
104	830728	46.07	122.74	15.65	2.3	176	3	79	68	244	46	106	52
106	830819	47.43	122.74	23.12	2.2	214	23	96	47	259	37	150	76
108	830901	47.77	122.72	19.20	2.5	163	0	73	30	212	69	114	69
110	830904	47.89	122.63	22.78	2.6	164	5	344	85	254	40	74	50
111	830914	47.09	121.93	19.02	2.2	161	60	295	22	353	29	220	69
113	830929	47.34	122.72	27.12	2.7	184	2	276	40	312	61	57	65
115	831023	46.56	122.35	17.28	2.5	212	7	111	58	272	47	147	59
119	831216	47.34	122.03	12.91	3.0	214	8	305	10	350	77	80	89
120	840104	47.68	122.58	18.83	2.8	216	13	119	28	261	60	165	80
122	840111	46.91	121.64	5.94	2.2	202	28	105	13	240	61	336	80
124	840219	47.35	122.35	15.83	2.4	160	10	347	80	249	35	71	55
126	840314	47.84	122.36	22.68	2.7	170	4	350	86	260	41	80	49
127	840323	47.75	122.69	19.07	2.9	174	0	84	0	39	90	309	90
131	840427	47.65	122.03	9.77	2.9	147	0	57	13	193	81	101	81
132	840602	47.49	122.71	21.49	3.6	216	4	308	22	350	72	84	78
133	840602	47.50	122.72	22.60	2.8	26	8	290	38	75	58	332	70
135	840619	47.72	122.99	8.78	3.0	0	0	90	0	315	90	45	90
139	840724	47.77	122.45	21.28	2.7	4	7	118	73	111	40	261	54
143	840905	47.92	122.04	17.37	2.2	322	5	212	76	38	42	244	51
146	840920	47.55	122.34	26.52	2.7	26	4	293	37	76	62	333	68
148	841029	47.85	122.43	18.35	2.0	168	3	264	62	284	49	54	54
151	841120	47.95	121.98	16.64	2.0	310	13	212	30	355	59	258	79
153	841130	47.76	122.24	23.72	2.7	178	28	85	6	218	66	315	75
154	841204	46.55	122.37	19.94	1.7	228	29	137	2	268	68	6	72
156	841220	47.88	122.46	22.65	2.2	5	5	102	54	127	51	246	59
157	850121	46.91	122.02	12.80	2.7	176	3	296	84	272	42	81	48
158	850123	47.77	122.47	18.39	2.6	181	6	295	75	285	41	79	52
159	850123	47.83	122.48	18.44	2.2	177	6	300	79	277	40	79	52
160	850129	47.48	121.83	17.55	2.7	359	3	262	67	67	47	289	52
163	850321	47.64	122.22	7.86	3.0	160	12	257	29	295	60	31	79
164	850330	46.70	122.20	15.98	2.8	148	21	246	21	287	60	197	90
165	850330	46.69	122.20	16.69	2.6	155	0	65	0	20	90	290	90
167	850417	47.70	122.25	23.94	1.9	184	18	297	50	314	40	68	71
169	850426	48.41	122.31	18.21	3.0	182	35	2	55	272	10	92	80
170	850430	48.40	122.32	18.16	2.4	32	0	302	0	257	90	167	90
172	850509	46.57	121.84	9.84	2.7	196	1	14	89	286	44	106	46
176	850616	47.44	121.87	17.03	3.1	314	6	49	37	84	60	187	69
177	850621	46.51	122.37	20.02	1.8	212	40	310	9	359	56	255	70
178	850706	47.77	122.27	17.97	3.1	157	13	54	44	206	49	98	70
182	850914	47.43	122.38	19.85	3.0	334	15	240	14	17	69	107	89
183	851006	47.93	122.90	19.96	2.8	322	0	52	70	71	48	213	48
184	851014	46.37	122.68	20.16	1.5	32	12	134	44	162	50	270	70
185	851017	47.46	123.00	15.87	2.6	178	0	268	67	289	49	67	49
186	851106	46.89	121.99	7.61	2.3	3	12	248	64	66	39	292	61
191	851227	46.97	121.94	7.02	3.0	346	3	255	19	32	74	299	79

TABLE A.2 - MT. ST. HELENS EARTHQUAKES

#	Date	Lat	Lon	Depth	Mag	P-axis		T-axis		Plane A		Plane B	
						az.	pl.	az.	pl.	az.	pl.	az.	pl.
16	820123	46.39	122.28	9.45	2.9	40	0	130	0	355	90	85	90
18	820127	46.42	122.26	8.09	2.1	43	16	155	53	170	41	288	68
19	820208	46.52	122.28	4.02	2.3	246	4	342	57	6	50	129	57
20	820217	46.41	122.32	10.61	1.7	34	0	124	0	349	90	79	90
21	820301	46.40	122.30	10.97	2.7	35	34	151	33	184	38	94	90
22	820301	46.42	122.30	11.33	1.8	212	19	108	35	255	50	157	80
23	820301	46.40	122.30	11.48	1.0	44	4	136	22	178	72	272	78
24	820302	46.39	122.30	11.40	2.0	40	20	143	33	178	51	274	82
25	820302	46.41	122.29	11.61	1.8	213	3	307	50	337	55	91	60
27	820303	46.39	122.30	11.13	1.5	20	4	110	4	155	84	65	90
28	820306	46.38	122.28	11.24	2.6	28	28	134	27	171	49	81	89
32	820316	46.41	122.33	12.65	1.7	24	4	291	34	73	64	333	70
33	820316	46.40	122.27	11.22	2.1	33	0	123	0	348	90	78	90
34	820320	46.39	122.33	11.60	2.4	208	21	306	20	347	60	257	89
35	820326	46.40	122.31	11.61	1.9	47	35	166	34	197	36	108	90
36	820401	46.38	122.25	11.94	2.2	38	12	135	30	173	60	270	78
37	820402	46.27	122.29	10.90	1.2	56	6	147	7	191	81	282	89
39	820410	46.38	122.31	8.88	2.2	240	40	144	8	274	57	18	69
40	820412	46.38	122.28	12.01	2.0	35	0	125	0	350	90	80	90
42	820417	46.37	122.25	9.14	1.7	45	0	135	0	0	90	90	90
43	820426	46.43	122.26	9.69	2.7	201	14	299	29	336	59	73	80
44	820521	46.41	122.07	2.92	1.5	75	75	255	15	345	30	165	60
45	820526	46.41	122.31	11.94	1.8	35	0	125	0	350	90	0	90
46	820527	46.36	122.26	7.52	1.7	34	0	124	0	349	90	79	90
47	820528	46.40	122.32	11.56	1.7	45	0	135	0	0	90	90	90
48	820531	46.39	122.32	12.04	3.0	42	20	139	19	181	62	91	90
49	820531	46.40	122.28	11.76	1.8	27	32	139	31	173	42	83	90
50	820605	46.43	122.29	10.44	1.5	298	65	116	25	204	20	27	70
51	820606	46.41	122.25	10.86	1.0	45	0	135	0	0	90	90	90
52	820606	46.38	122.25	5.45	1.4	45	0	135	0	0	90	90	90
53	820704	46.35	122.30	9.26	1.2	212	33	328	34	359	39	90	89
54	820712	46.30	122.30	11.45	1.1	45	0	135	0	0	90	90	90
56	820724	46.31	122.26	9.25	1.2	18	14	284	14	61	70	156	90
57	820819	46.40	122.25	9.68	2.3	38	20	136	20	177	61	267	90
59	821008	46.28	122.08	0.77	2.2	168	75	348	15	78	30	258	60
60	821009	46.39	122.31	8.91	1.7	58	26	312	29	96	49	5	88
64	821113	46.39	122.29	10.97	1.8	62	47	318	12	87	48	198	69
65	821116	46.31	122.30	10.58	1.9	38	0	128	0	353	90	83	90
66	821128	46.34	122.28	11.93	2.6	13	23	126	43	150	41	254	78
68	821212	46.38	122.30	14.80	2.2	26	5	116	4	161	84	71	89
69	821212	46.28	122.50	15.85	1.9	8	13	98	0	144	81	52	81
74	830129	46.36	122.34	11.50	1.3	154	5	248	36	285	61	26	69
77	830208	46.44	122.33	9.25	1.2	40	13	133	12	177	72	86	89
79	830309	46.40	122.29	11.36	1.1	200	35	299	12	345	56	245	75
82	830318	46.41	122.24	7.65	1.5	40	12	132	11	176	74	86	89
83	830320	46.12	122.13	9.12	2.0	207	5	299	22	341	71	75	78
86	830412	46.41	122.33	10.31	1.5	18	25	120	25	160	51	256	82
87	830412	46.39	122.31	8.61	2.0	32	30	123	1	171	68	73	70
88	830420	46.41	122.32	9.48	2.3	218	16	124	15	261	68	351	89
89	830420	46.41	122.33	9.27	2.3	38	10	130	11	174	75	264	89
93	830506	46.41	122.23	7.41	2.3	38	0	128	0	353	90	83	90
96	830519	46.39	122.30	8.98	1.5	40	18	136	18	178	64	268	90

TABLE A.2 - MT. ST. HELENS EARTHQUAKES (CONT.)

#	Date	Lat	Lon	Depth	Mag	P-axis		T-axis		Plane A		Plane B	
						az.	pl.	az.	pl.	az.	pl.	az.	pl.
98	830521	46.38	122.37	9.32	1.9	180	18	87	10	222	70	314	84
109	830902	46.33	122.53	15.94	1.0	49	45	306	13	76	49	185	70
112	830915	46.53	122.45	15.31	2.3	16	6	110	36	147	61	249	70
114	831002	46.46	122.33	9.20	2.2	38	0	128	28	169	71	267	71
117	831101	46.34	122.29	9.95	2.0	155	32	259	21	300	51	205	83
118	831213	46.37	122.26	9.42	1.8	238	15	332	16	15	68	105	89
123	840111	46.41	122.28	6.52	1.7	27	0	117	0	342	90	72	90
129	840404	46.43	122.32	9.21	2.4	24	10	135	64	141	41	274	59
138	840716	46.49	122.30	15.25	2.8	210	6	303	25	344	68	79	77
140	840805	46.52	122.32	11.26	3.1	22	20	290	6	64	71	157	80
144	840908	46.29	122.28	7.00	1.4	210	22	117	8	251	69	345	81
145	840915	46.50	122.40	13.36	1.1	26	12	119	12	162	73	72	90
147	841016	46.43	122.31	10.58	1.2	0	25	180	65	90	20	270	70
149	841103	46.41	122.32	11.24	1.9	0	25	180	65	90	20	270	70
150	841103	46.41	122.31	11.57	1.1	12	38	106	5	156	60	53	68
166	850414	46.40	122.25	8.03	2.1	25	8	291	26	71	66	335	78
171	850430	46.41	122.30	10.95	2.0	37	27	143	29	180	49	271	89
174	850523	46.21	122.21	0.72	2.5	190	0	10	90	100	45	280	45
179	850801	46.26	122.52	16.91	1.4	13	7	277	40	63	57	318	68
181	850905	46.33	122.23	7.16	2.5	9	11	101	11	145	74	55	90
188	851117	46.43	122.33	11.06	2.9	45	0	135	0	0	90	90	90

TABLE A.3 - SLAB EARTHQUAKES

#	Date	Lat	Lon	Depth	Mag	P-axis		T-axis		Plane A		Plane B	
						az.	pl.	az.	pl.	az.	pl.	az.	pl.
1	800204	47.39	121.65	96.35	2.4	55	85	236	5	326	40	146	50
2	800416	48.19	122.90	50.10	3.8	258	6	164	36	307	61	205	70
3	800608	47.97	123.10	48.54	4.2	272	84	15	1	99	44	291	47
4	800816	47.39	123.26	43.11	2.3	228	55	111	17	238	38	358	68
5	800906	47.54	123.42	46.16	2.8	173	68	62	8	175	41	315	56
6	801106	47.91	123.17	45.56	2.9	201	34	106	8	238	61	338	73
7	801130	47.35	123.34	43.81	2.6	130	20	32	20	171	61	81	90
8	810111	47.39	123.47	40.58	1.8	90	7	209	76	194	39	349	53
9	810704	47.86	122.73	52.11	2.8	303	31	47	22	88	51	353	84
10	810705	47.56	123.68	39.13	2.0	55	27	216	62	164	19	318	72
11	810722	47.96	123.43	44.18	2.3	227	64	89	20	205	29	346	67
12	810804	47.69	123.13	43.85	1.9	0	71	123	11	194	37	46	57
13	810821	47.62	123.67	40.52	2.8	180	85	0	5	90	40	270	50
15	820114	48.10	122.81	55.95	2.7	254	65	74	25	164	20	344	70
31	820313	47.06	122.17	72.53	1.9	266	45	86	45	356	90	176	90
62	821101	47.55	123.38	45.61	2.5	197	74	40	15	139	31	305	60
76	830205	46.67	123.04	52.22	2.2	158	65	43	11	159	39	295	60
91	830425	47.28	123.56	38.31	1.9	99	31	7	4	138	66	237	71
101	830708	47.76	123.02	47.12	2.4	144	55	281	27	332	25	208	75
105	830802	47.66	122.87	48.48	2.3	254	85	74	5	164	40	344	50
107	830828	48.00	122.87	51.50	3.9	75	16	345	0	119	79	211	79
116	831031	47.35	123.29	43.36	4.3	316	75	134	15	223	30	44	60
121	840105	47.44	122.28	38.77	1.9	108	4	287	86	198	41	18	49
125	840223	47.65	123.04	46.32	2.2	117	48	16	10	143	50	255	66
128	840328	47.33	123.13	42.89	1.9	136	50	249	18	299	40	185	71
130	840408	46.80	122.49	67.03	3.3	286	20	44	53	55	36	173	71
134	840604	46.29	123.04	52.60	3.7	184	31	88	10	221	61	319	76
136	840621	48.30	122.97	46.47	2.0	132	7	225	21	266	70	0	80
137	840708	47.57	122.81	46.69	2.2	307	35	128	55	35	10	217	80
141	840812	47.73	123.02	46.32	2.2	112	0	22	43	166	61	58	61
142	840902	48.75	123.20	57.01	2.6	317	12	137	78	47	33	227	57
152	841121	46.98	123.69	35.67	2.8	211	36	326	30	1	40	267	86
155	841217	47.31	122.91	46.30	3.2	236	29	131	25	272	50	4	88
161	850306	48.90	122.82	66.48	1.8	41	21	145	32	179	51	275	83
162	850318	47.37	122.64	53.30	3.5	276	34	20	20	63	50	326	81
168	850426	47.31	122.48	57.83	2.5	271	12	170	42	320	52	214	71
173	850521	47.66	123.22	47.22	2.8	113	22	213	24	253	56	344	89
175	850523	47.67	123.31	47.04	2.0	33	6	125	21	167	71	261	80
180	850822	47.67	122.91	50.27	1.8	244	25	62	65	336	20	153	70
187	851115	47.51	123.59	42.13	2.7	270	76	90	14	180	31	0	59
189	851202	49.06	123.58	59.40	2.3	173	62	60	12	179	40	310	61
190	851204	48.86	122.87	59.14	2.2	240	60	22	24	81	25	305	71

FIGURE CAPTIONS

Fig. 1. Cross section showing hypocenters of earthquakes used in this study projected onto EW plane. Dashed line shows approximate top of subducted Juan de Fuca plate.
Fig. 2. Epicenter map of all crustal earthquakes in focal mechanism data set. The box in the Mt. St. Helens region was used for event selection.
Fig. 3. Focal mechanisms of 17 larger magnitude (M 3.0) crustal earthquakes used in this study. See text for discussion.
Fig. 4. Composite plots of P (left) and T (right) axes for the 76 shallow Puget Sound data set.
Fig. 5. Composite plots of P (left) and T (right) axes for the 73 event St. Helens region data set.
Fig. 6. Epicenter map for all subcrustal (intraslab) earthquakes.
Fig. 7. Focal mechanisms of 8 larger intraslab earthquakes. This figure illustrates the variability of focal mechanisms within the intraslab suite.
Fig. 8. Composite plots of P (left) and T (right) axes for the 42 subcrustal (intraslab) earthquakes plotted in Fig. 6.
Fig. 9. Results of stress inversion for 76 shallow Puget Sound earthquakes using Gephart and Forsyth's method. The best fitting model is listed in Table 1. The left figure shows the distribution of allowed P axes for 50% confidence limit, and the right figure shows P axes for 95% confidence limit.
Fig. 10. Result of stress inversion for 73 Mt. St. Helens earthquakes. Layout is the same as for Figure 9.
Fig. 11. Results of stress inversion for 42 subcrustal earthquakes. Layout is the same as for Figure 9.
Fig. 12. T axes of the slab earthquakes projected onto a NS cross section. The labeled curves are approximate contours at equal longitudes from the model of Crosson and Owens (1987).
Fig. 13. P axes for the slab earthquakes in a plot with the same layout as Figure 12.
Fig. A.1. Focal mechanisms of shallow Puget Sound earthquakes.
Fig. A.2. Focal mechanisms of Mt. St. Helens earthquakes.
Fig. A.3. Focal mechanisms of slab earthquakes.

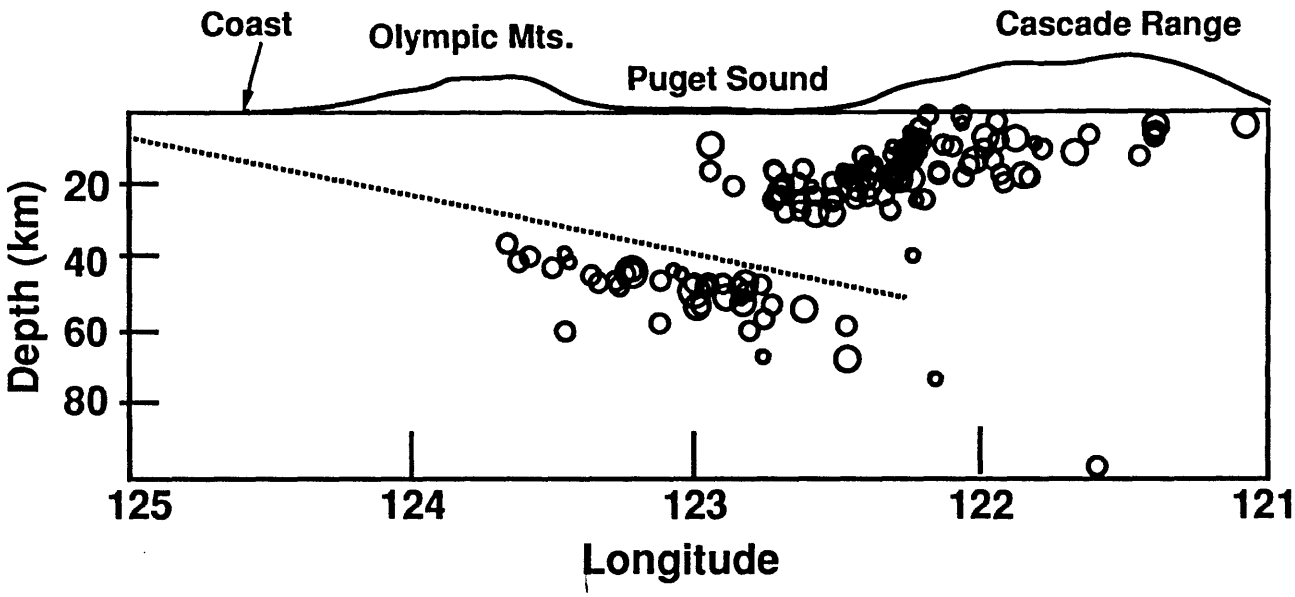
Coast
Olympic Mts.
Puget Sound
Cascade Range
Depth (km)
20
40
60
80
125
124
123
122
121
Longitude

Figure 1

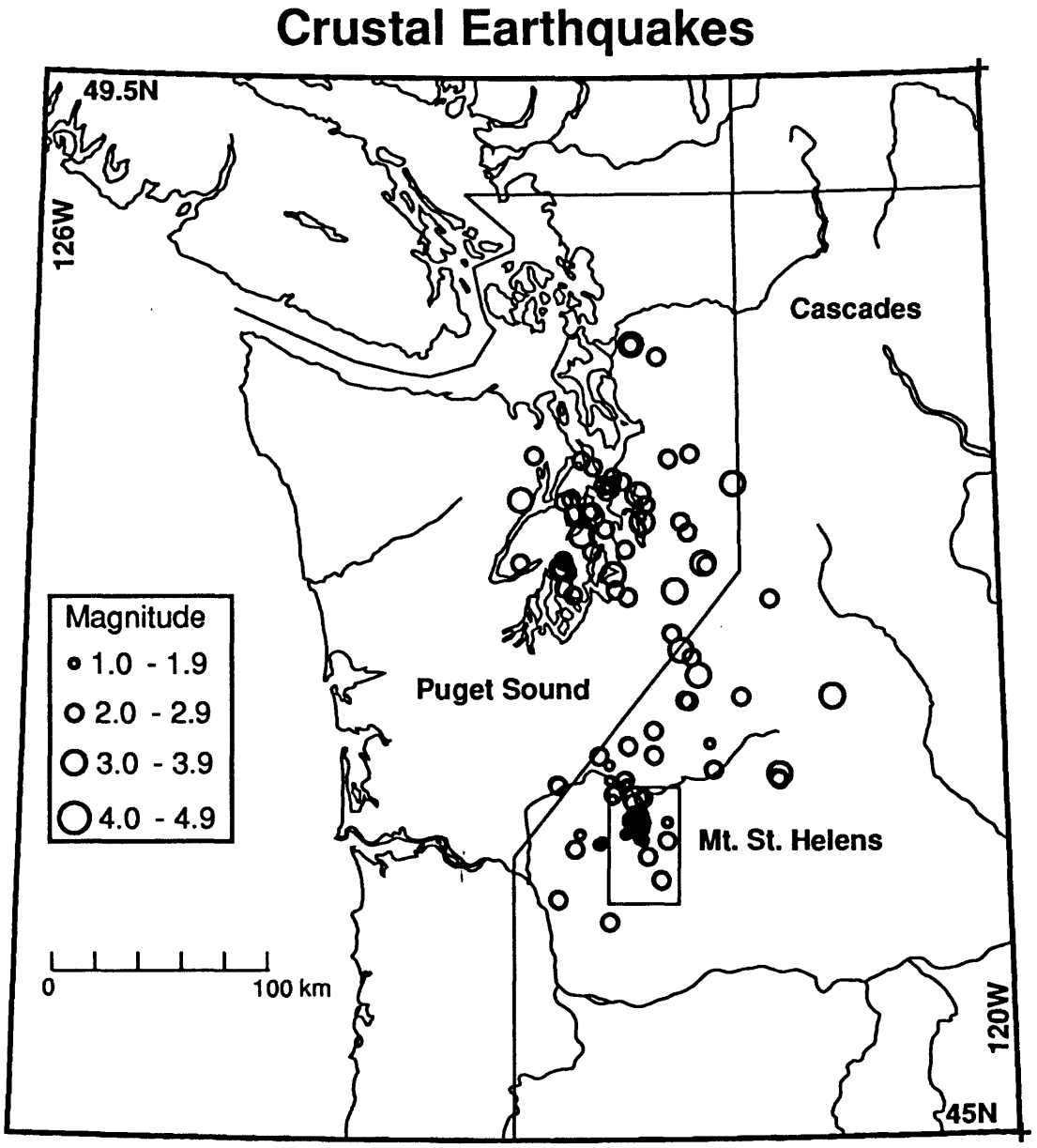
Crustal Earthquakes
49.5N
126W
Cascades
Puget Sound
Mt. St. Helens
Magnitude
1.0 - 1.9
2.0 - 2.9
3.0 - 3.9
4.0 - 4.9
0
100 km
120W
45N

Figure 2

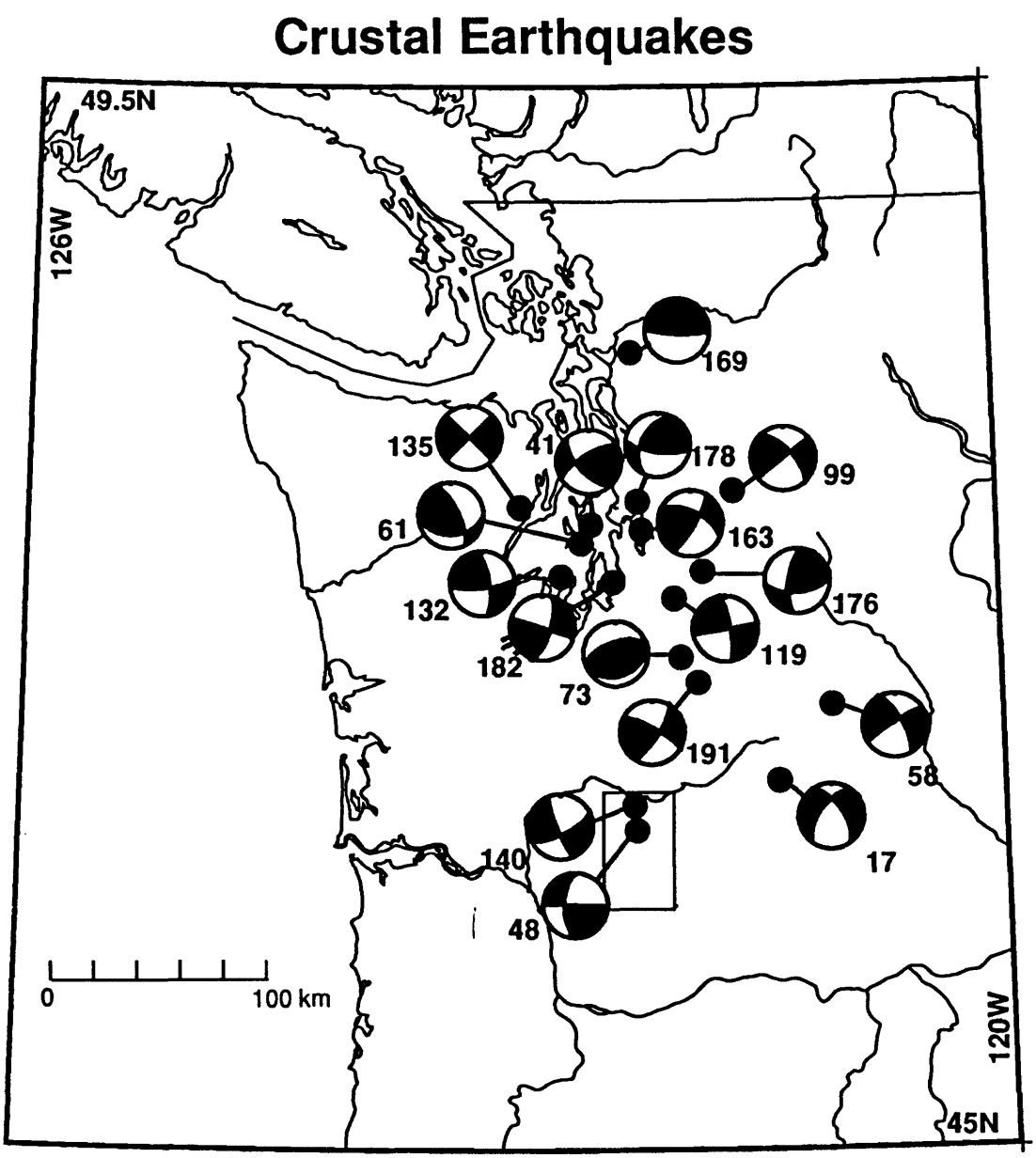
Crustal Earthquakes
49.5N
126W
169
135
41
178
99
61
163
132
176
182
119
73
191
58
17
140
48
0
100 km
120W
45N

Figure 3

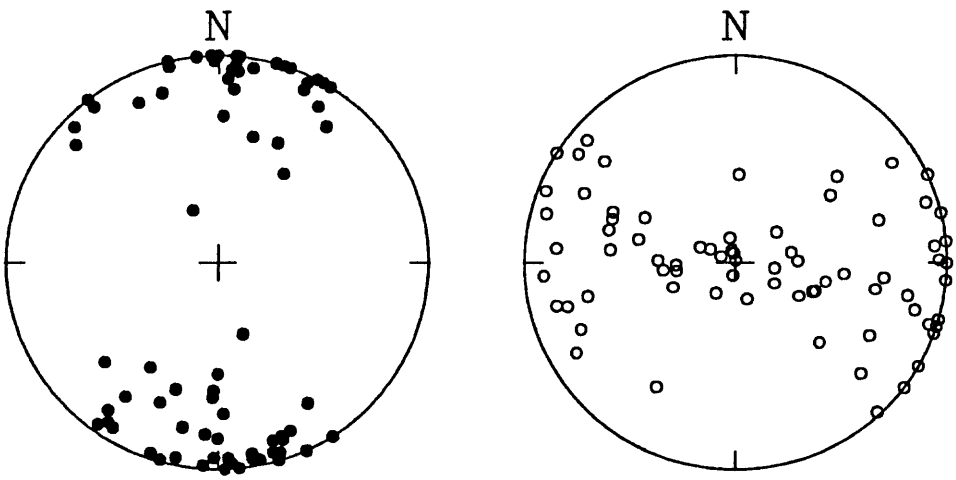

Figure 4

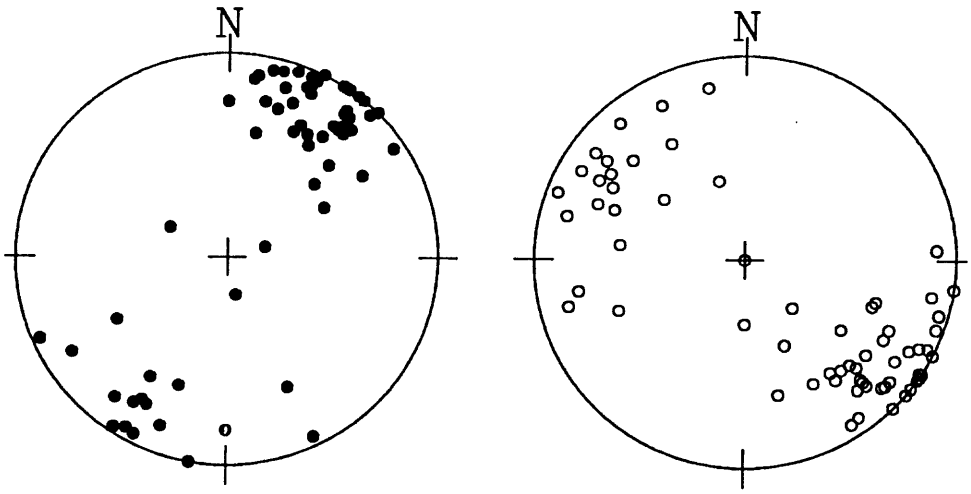

Figure 5

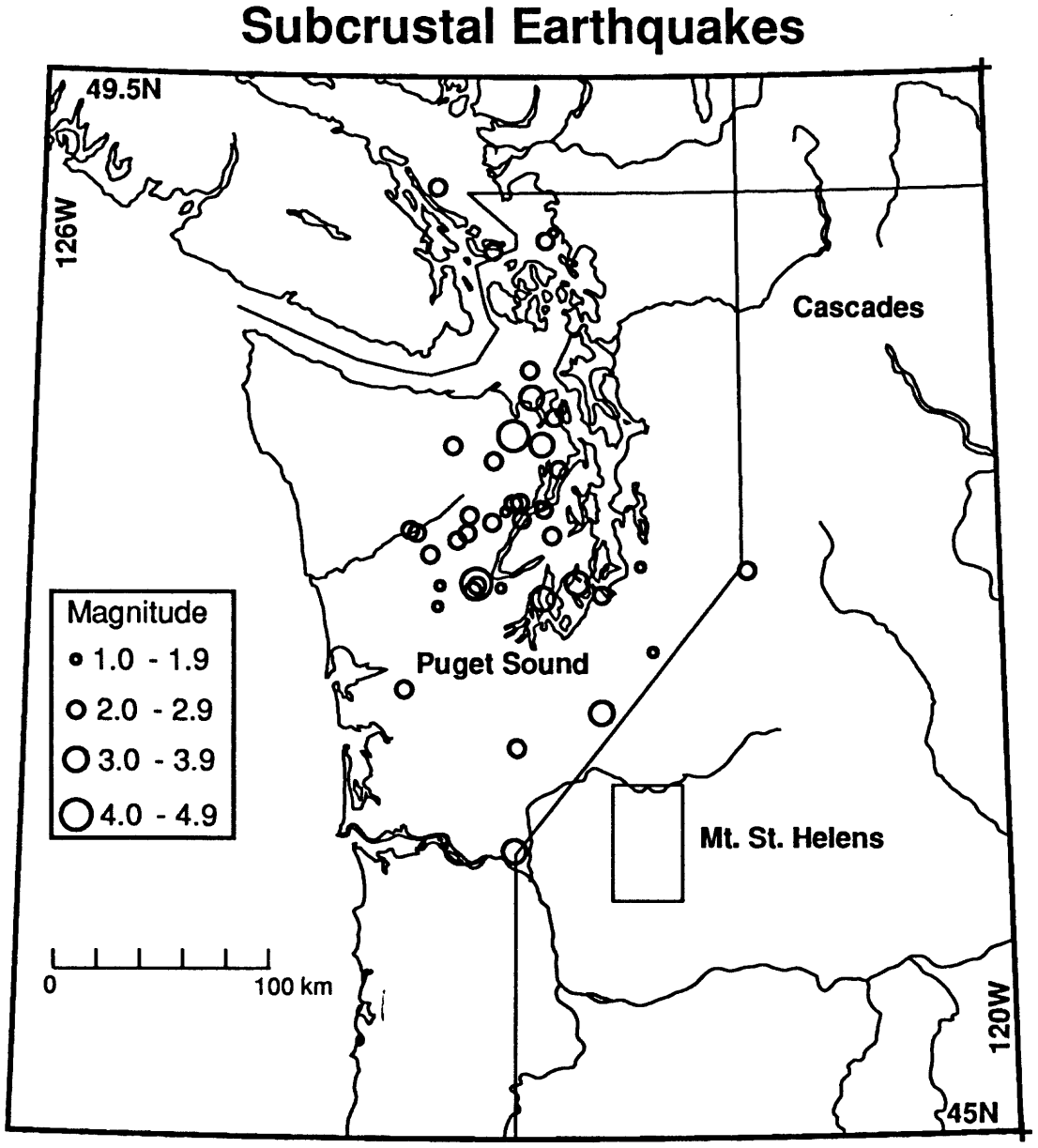
Subcrustal Earthquakes
49.5N
126W
Cascades
Magnitude
1.0 - 1.9
2.0 - 2.9
3.0 - 3.9
4.0 - 4.9
Puget Sound
Mt. St. Helens
0
100 km
120W
45N

Figure 6

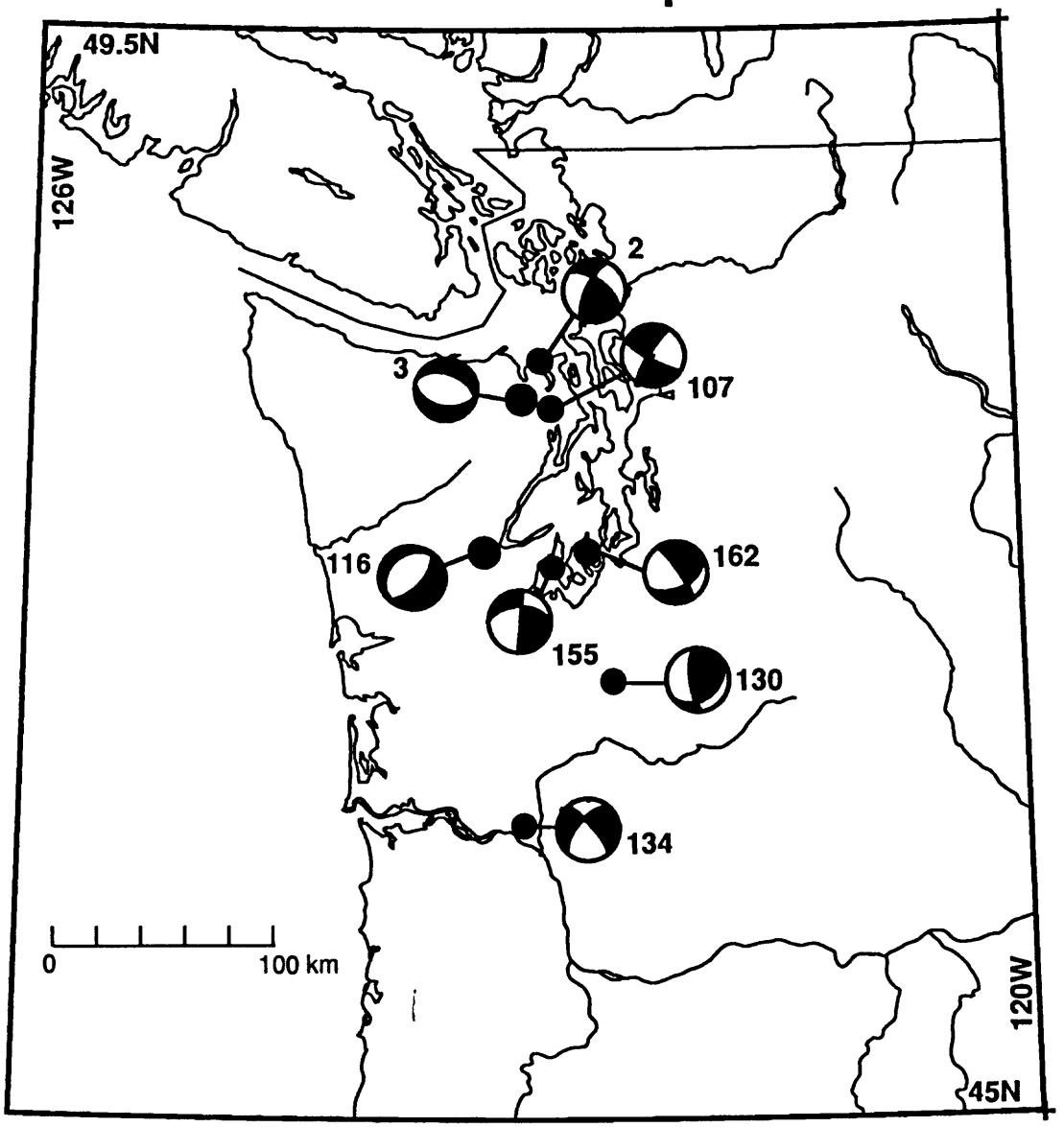
Subcrustal Earthquakes
49.5N
126W
2
3
107
116
162
155
130
134
0
100 km
120W
45N

Figure 7

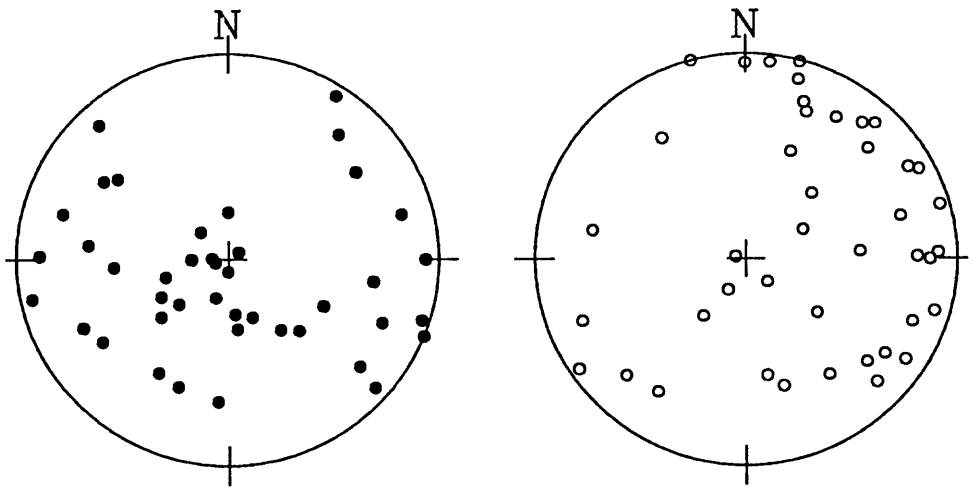

Figure 8

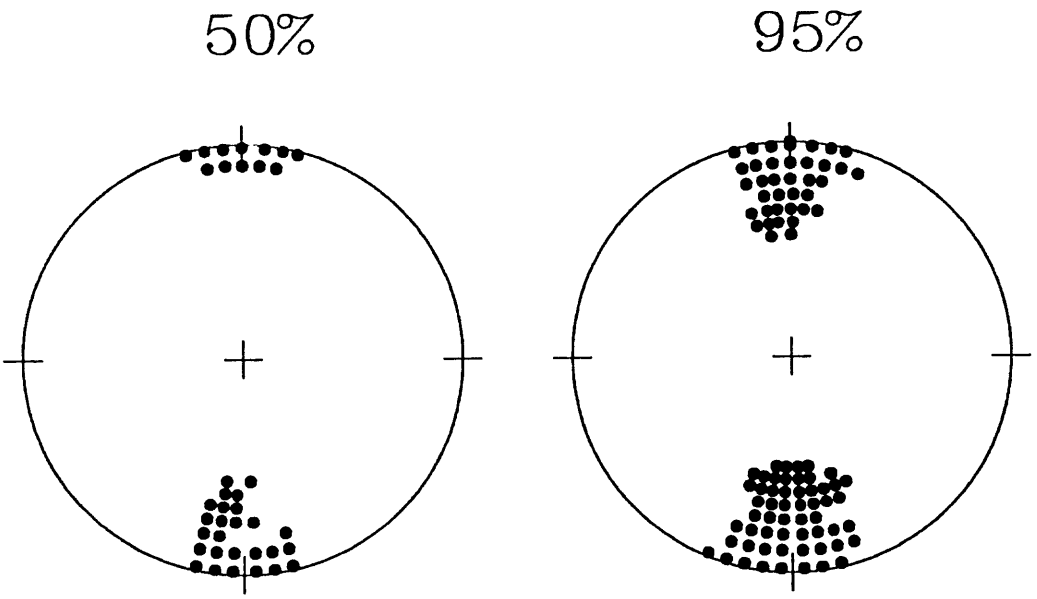

Figure 9

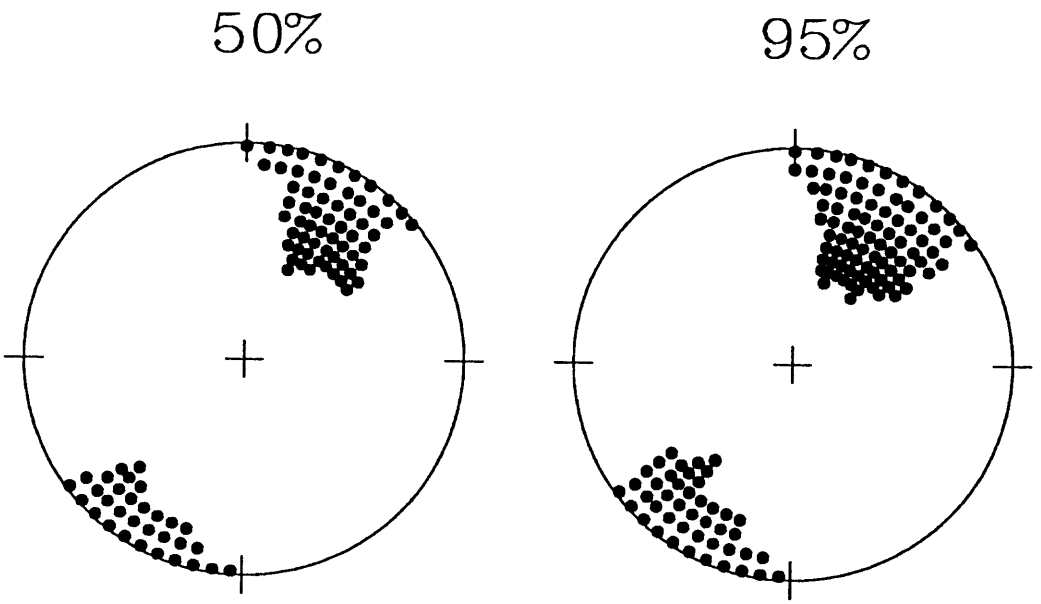

Figure 10

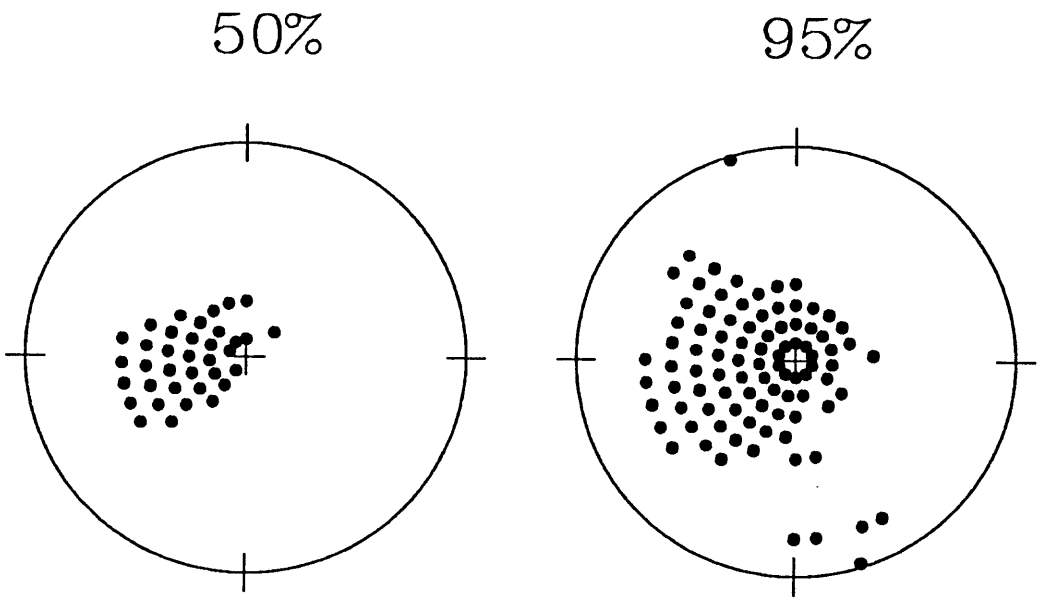

Figure 11

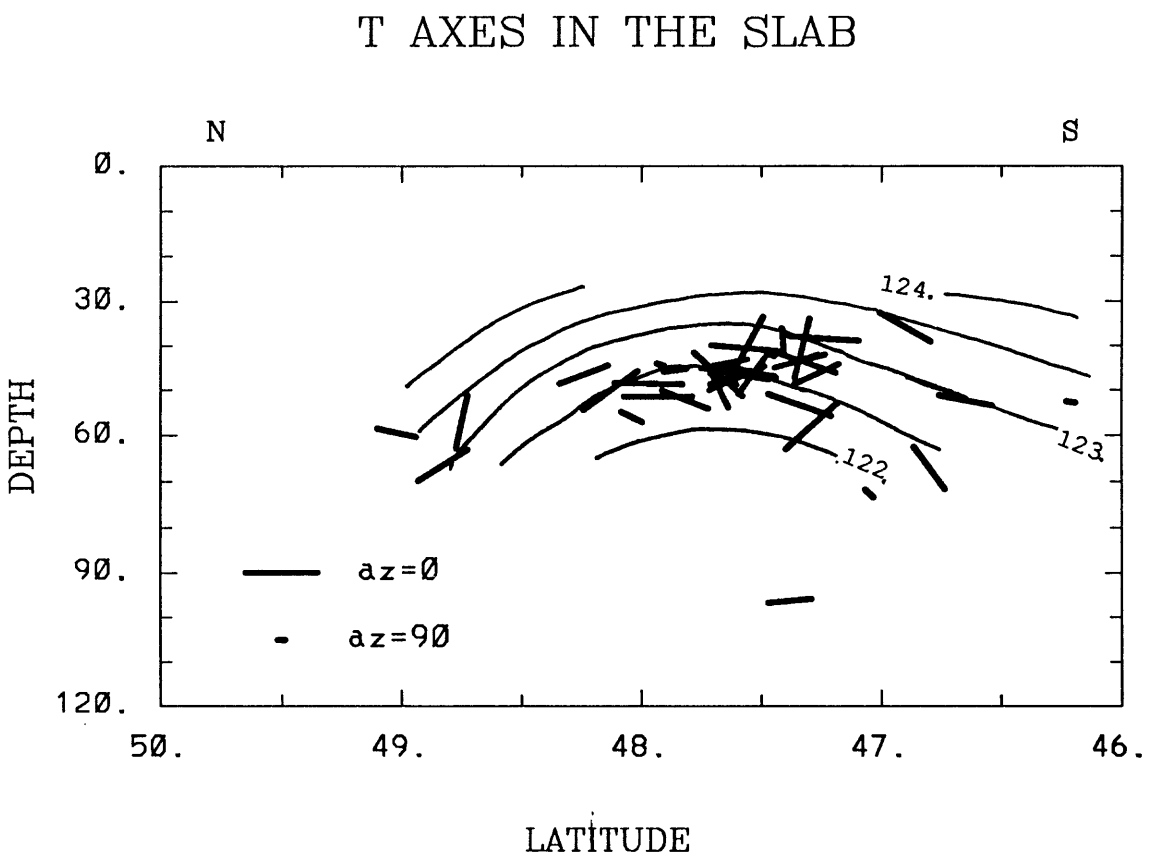
T AXES IN THE SLAB
N
S
0.
30.
60.
90.
120.
DEPTH
124.
123.
122.
az=0
az=90
50.
49.
48.
47.
46.
LATITUDE

Figure 12

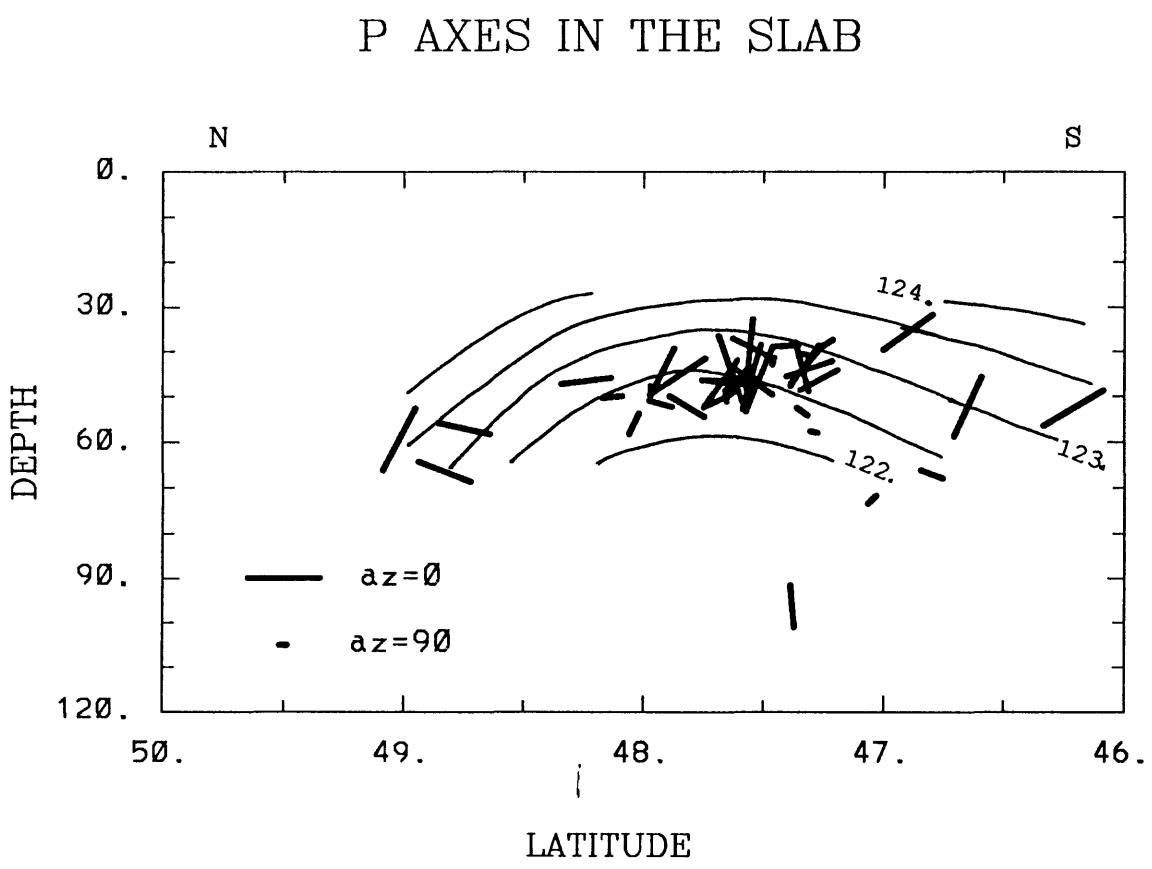
P AXES IN THE SLAB
N
S
0.
30.
60.
90.
120.
DEPTH
124.
123.
122.
az=0
az=90
50.
49.
48.
47.
46.
LATITUDE

Figure 13

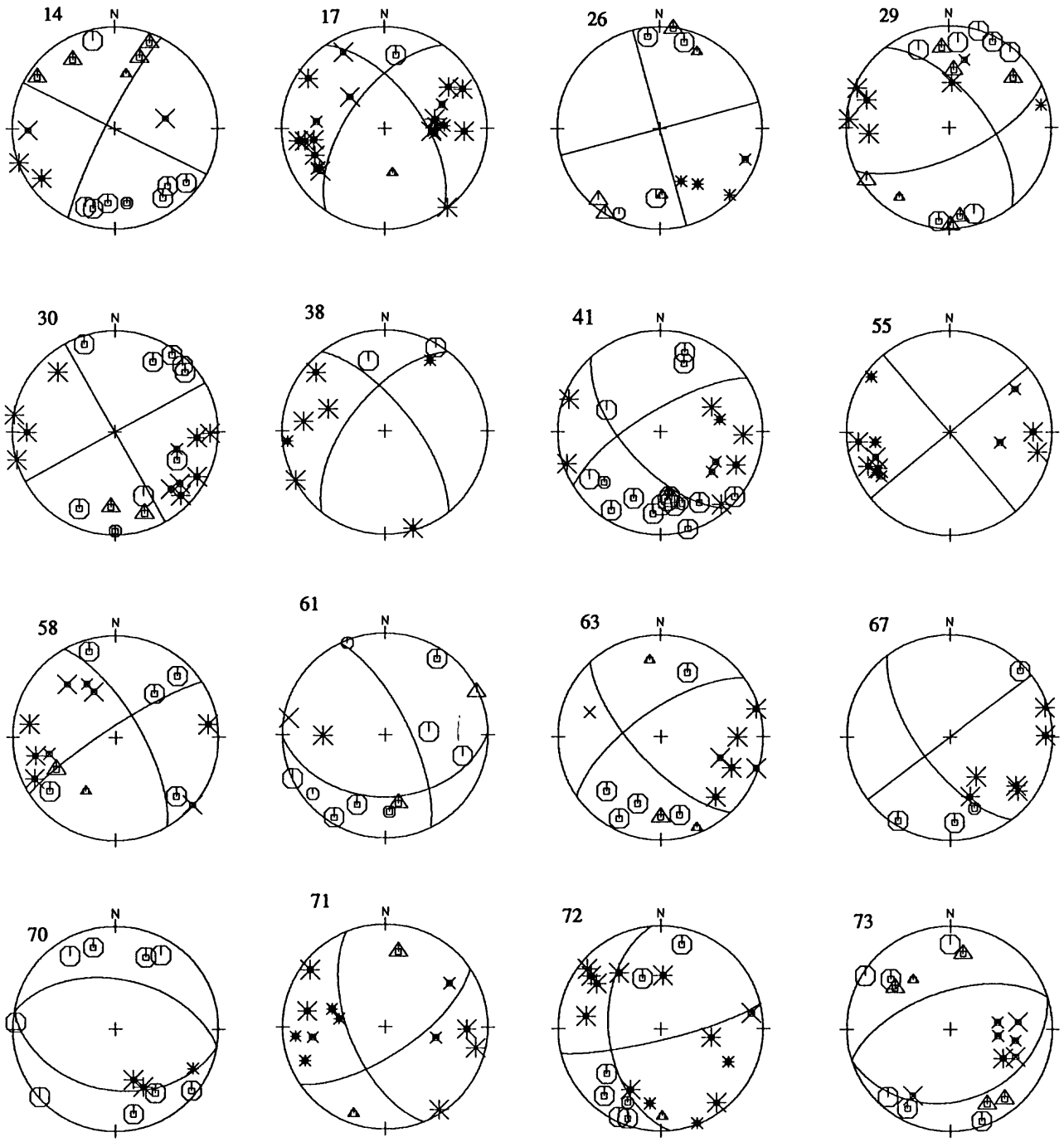

Figure A.1

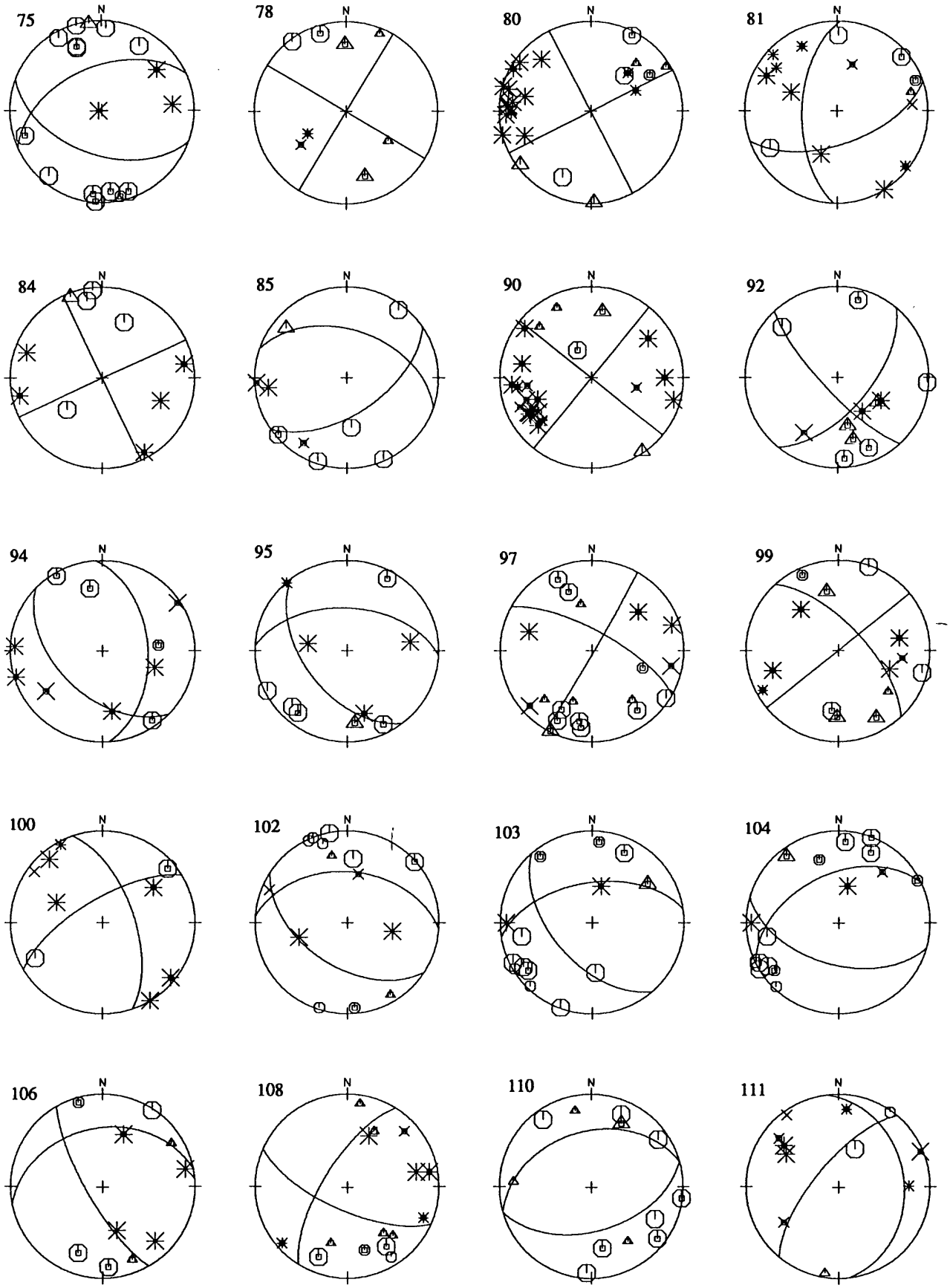

Figure A.1--Continued

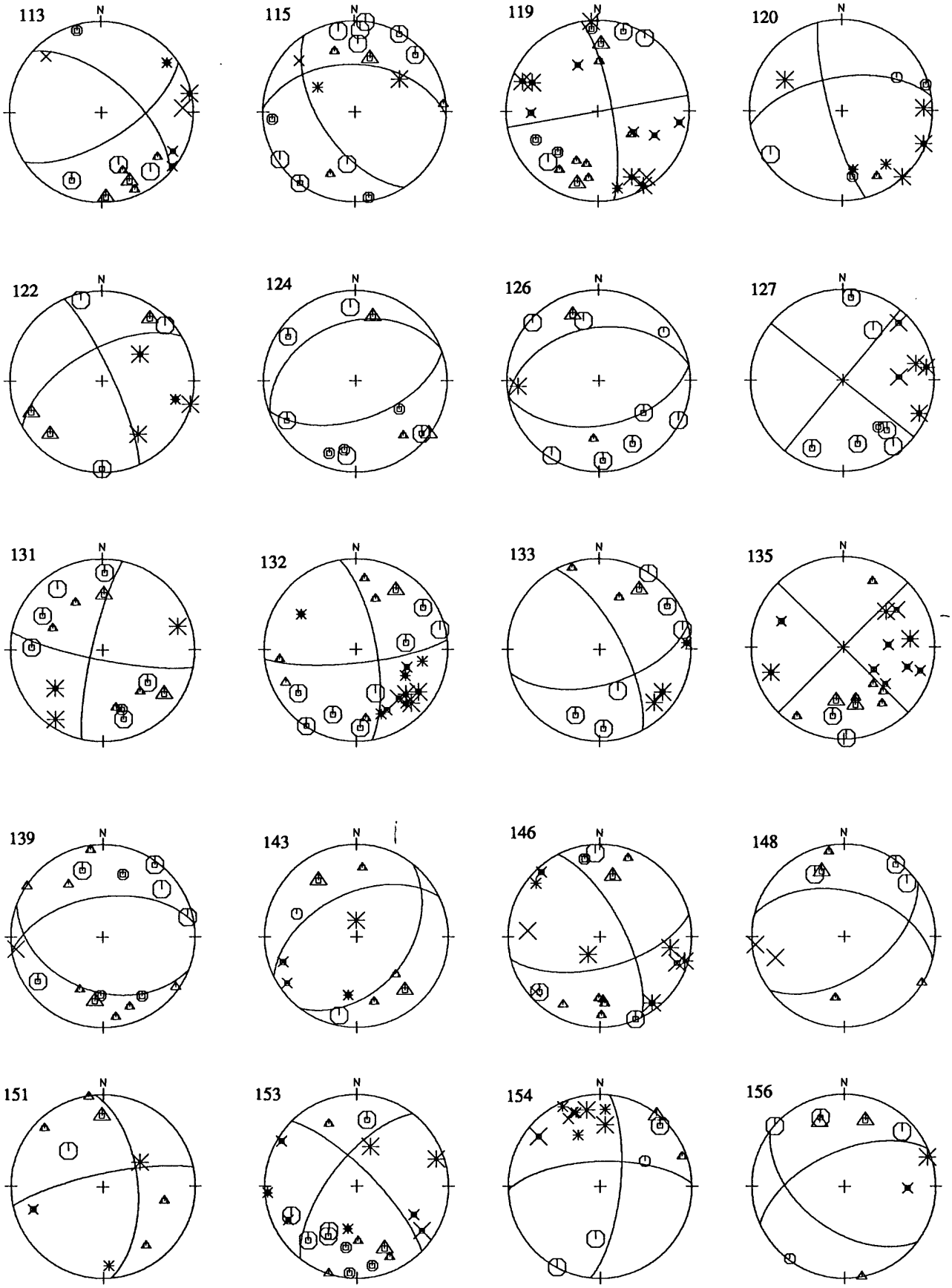

Figure A.1--Continued

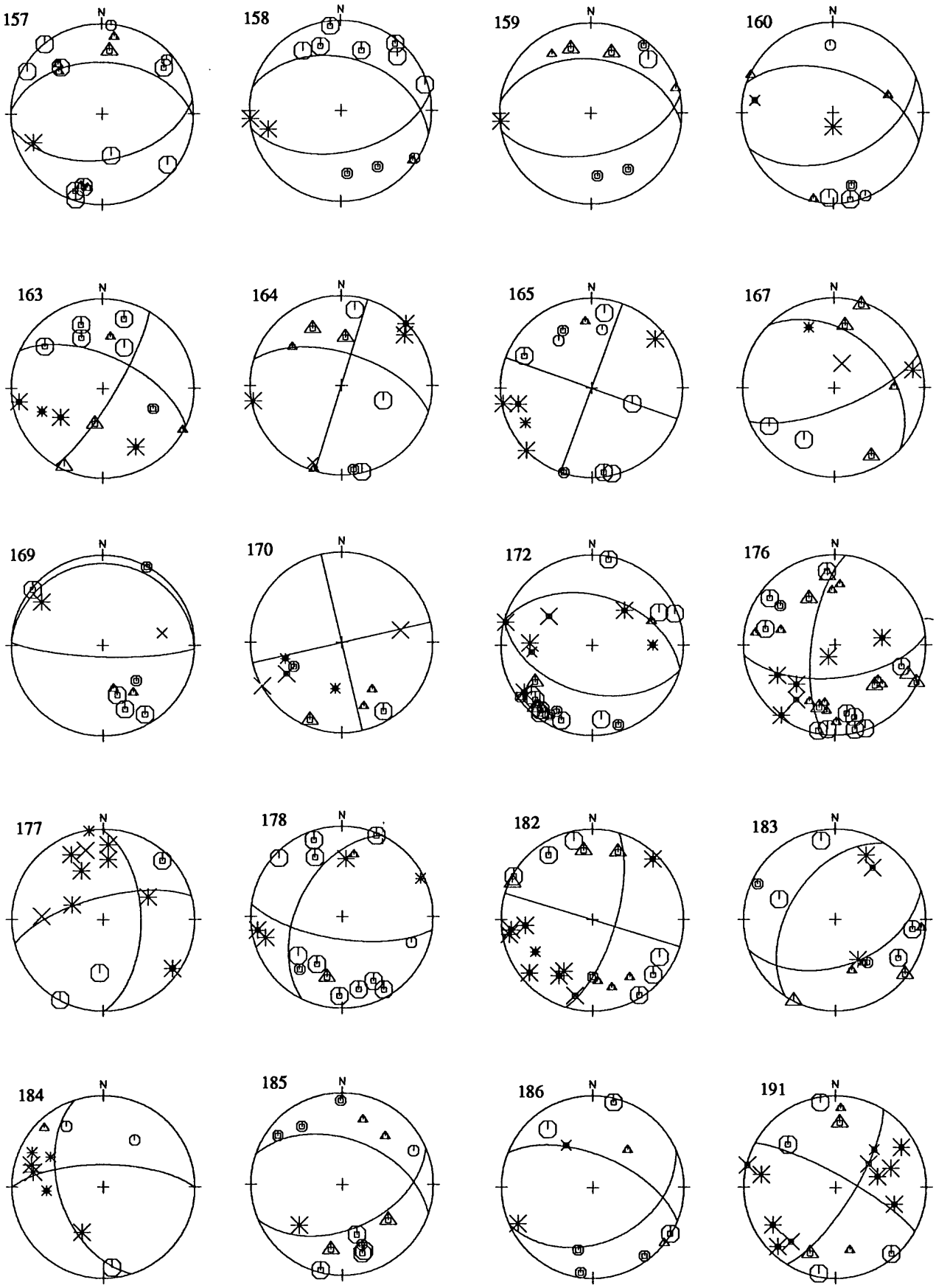

Figure A.1--Continued

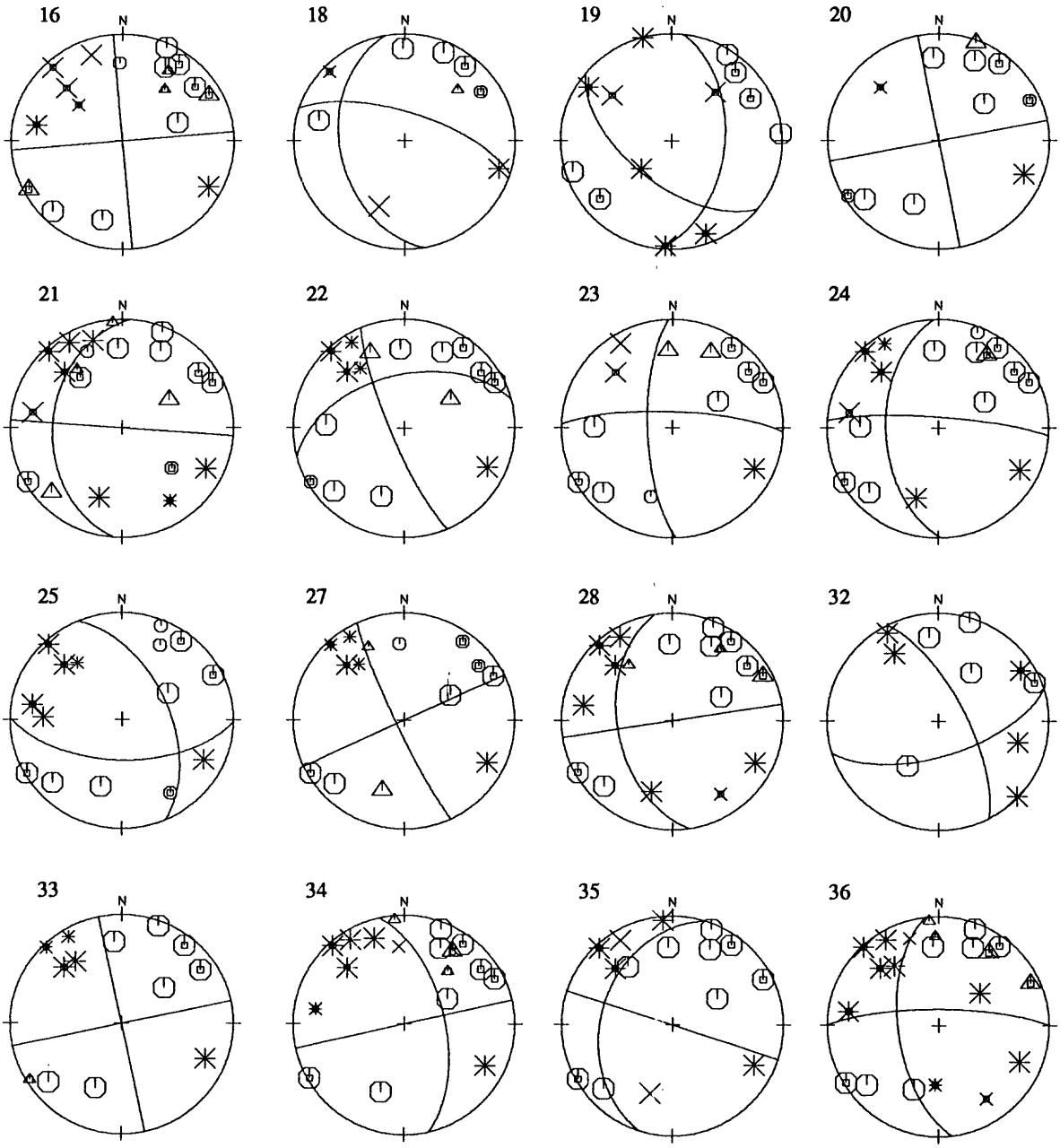

Figure A.2

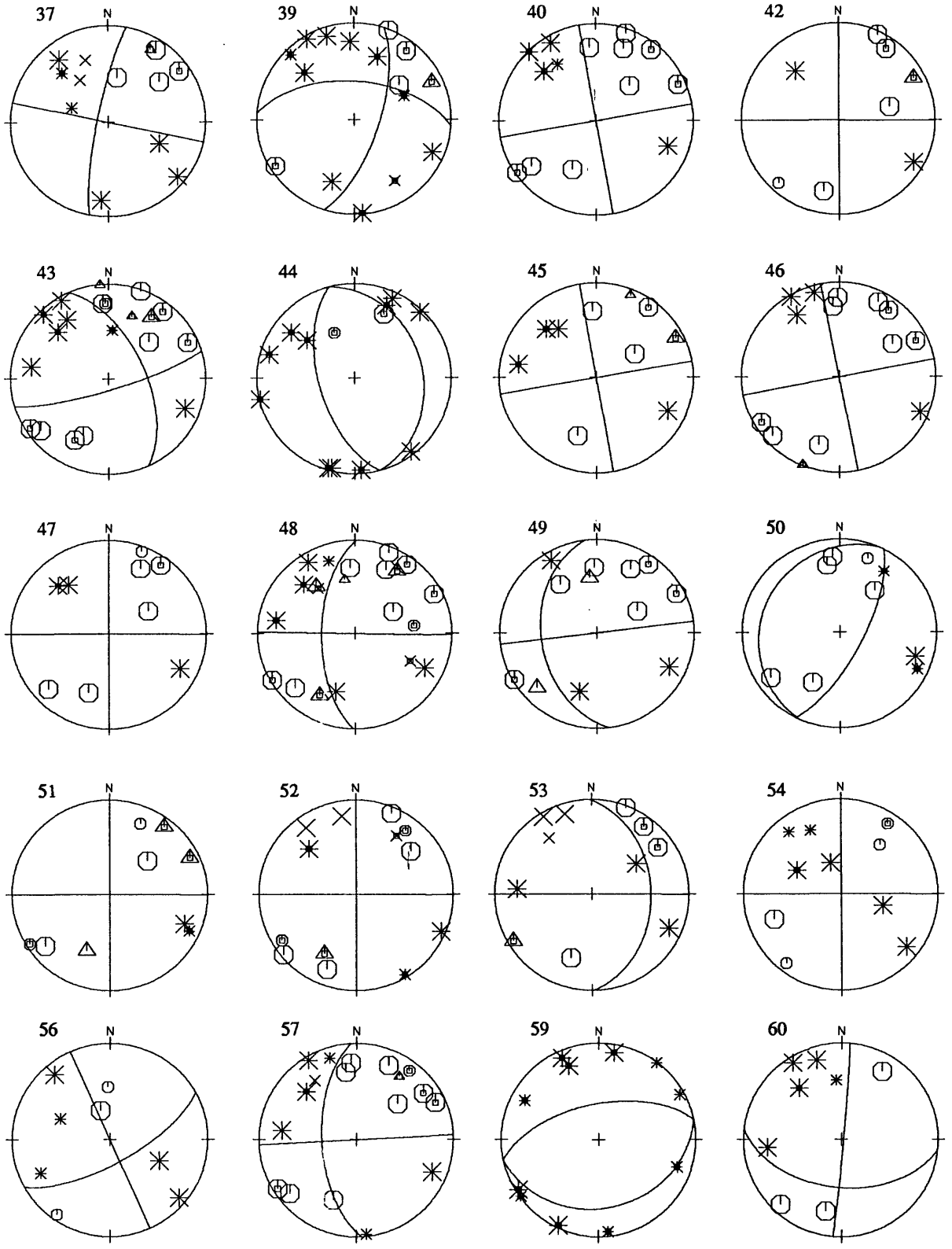

Figure A.2--Continued

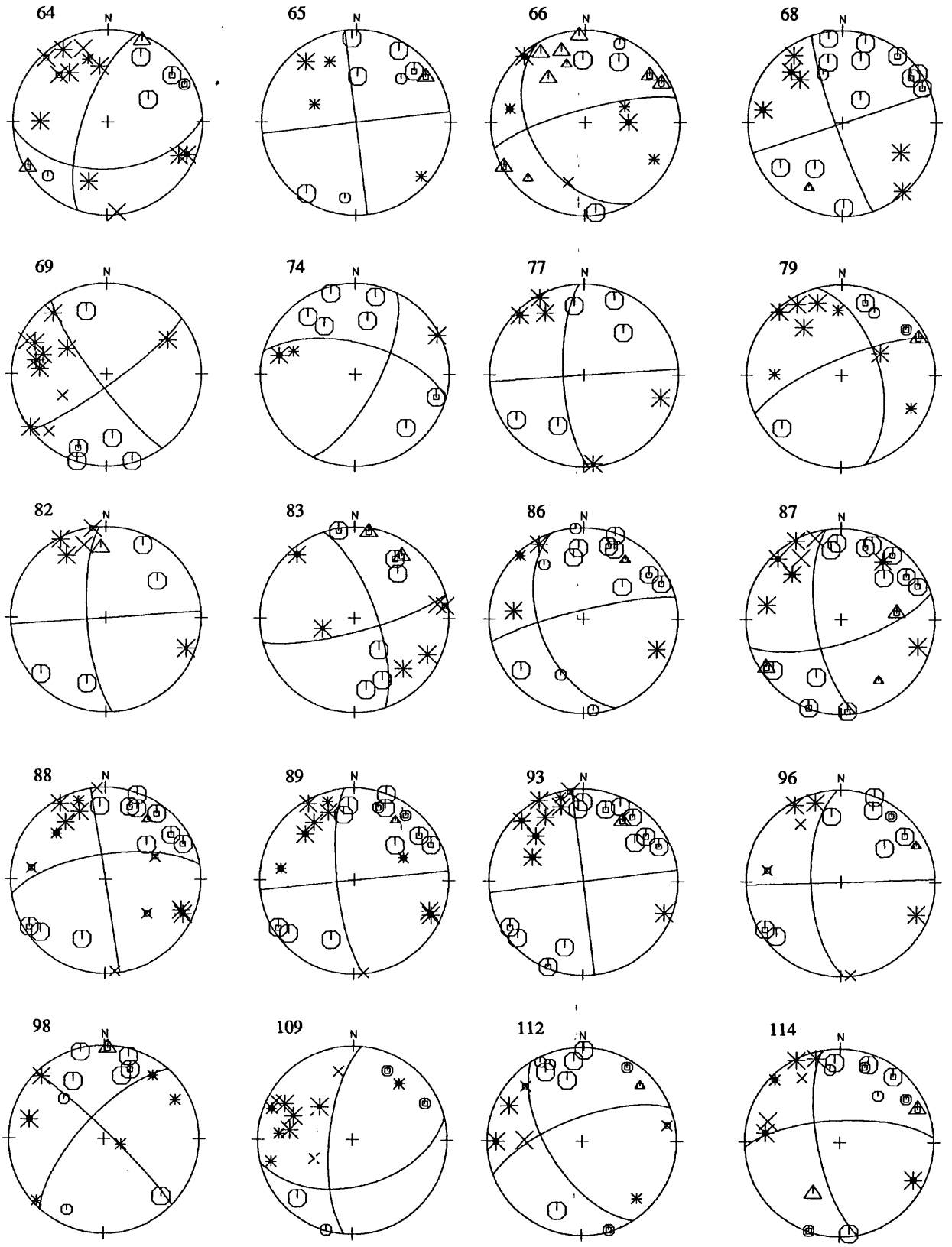

Figure A.2--Continued

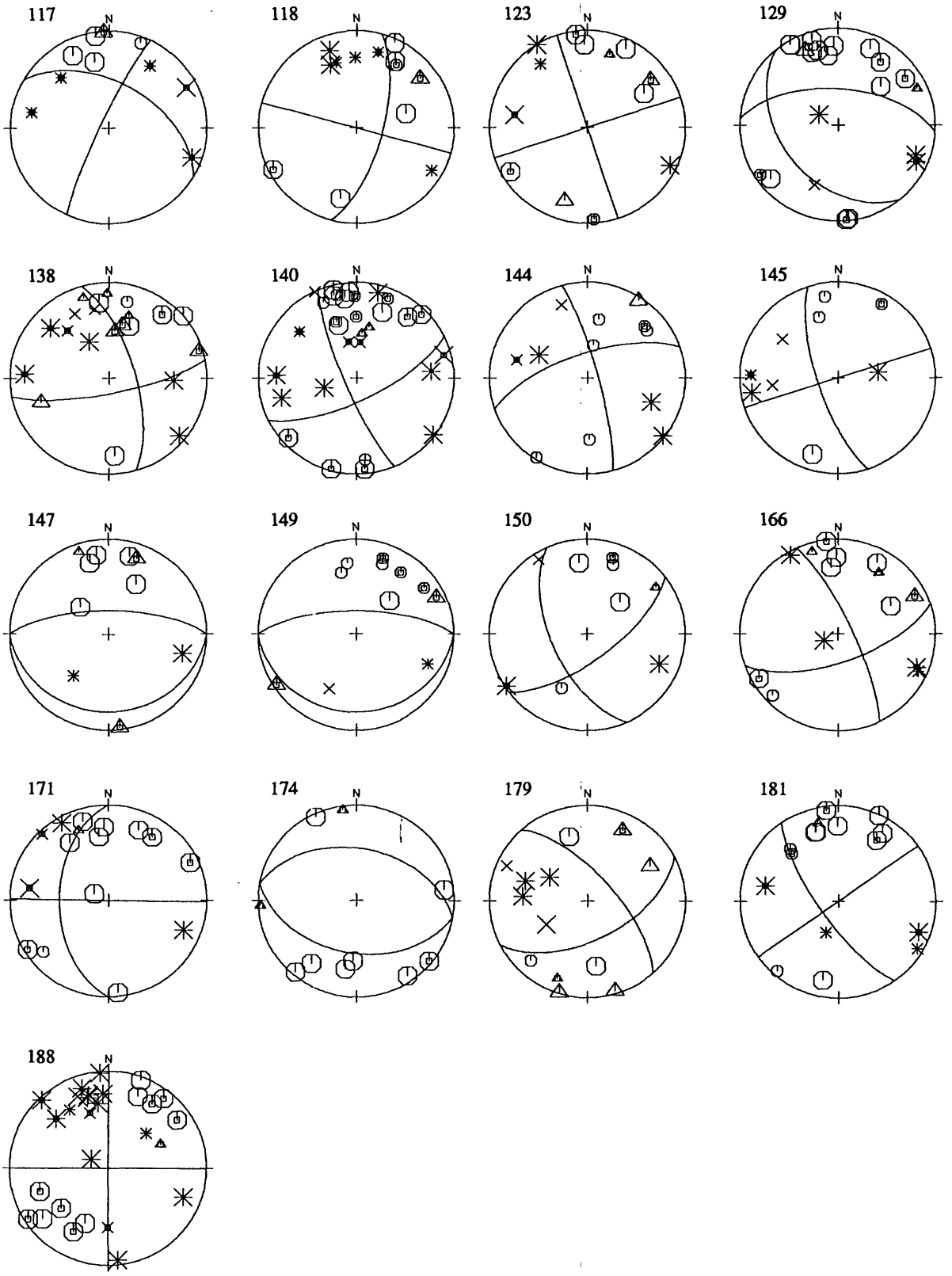

Figure A.2--Continued

Slab Earthquakes

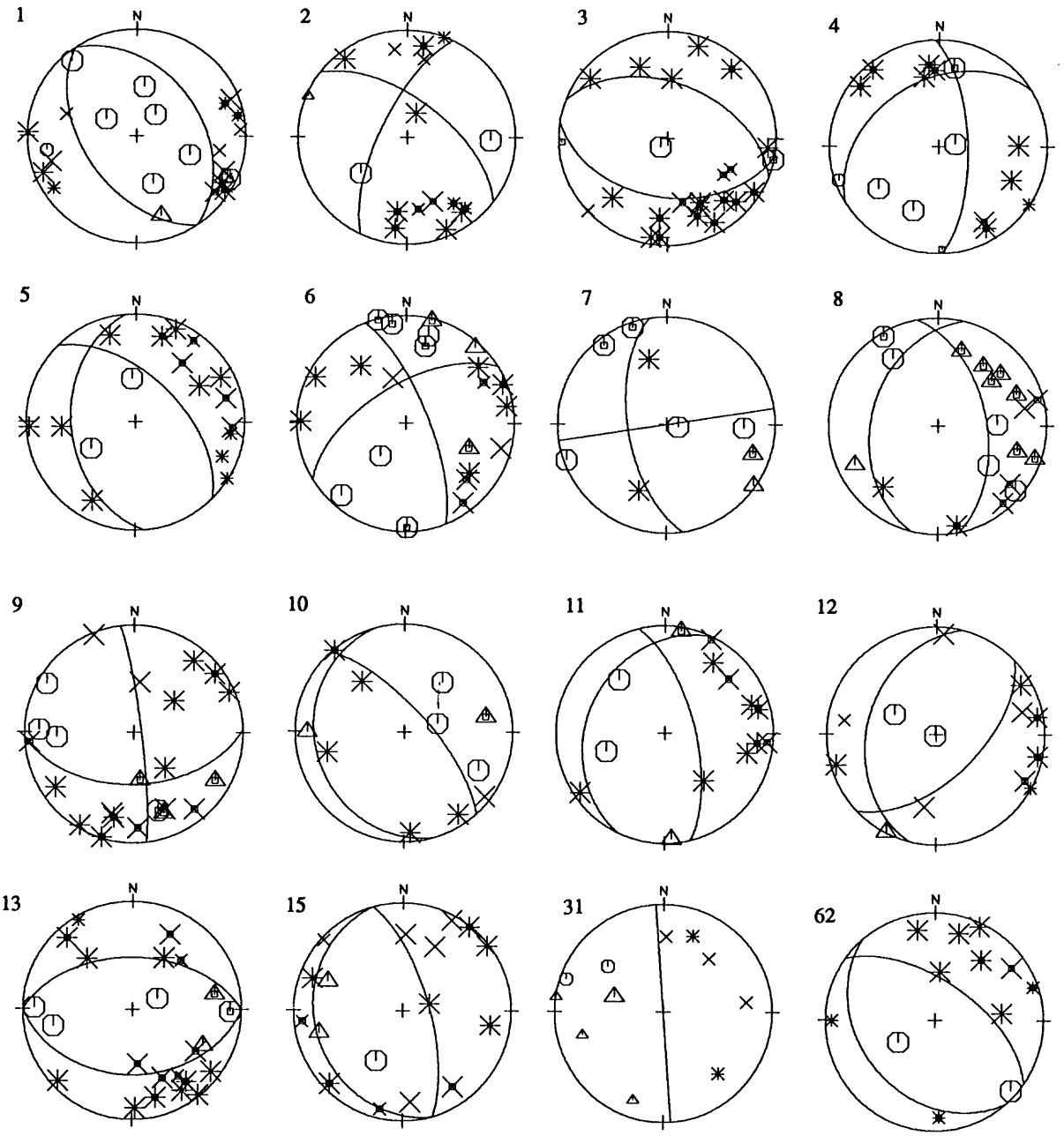

Figure A.3

Slab Earthquakes - cont.

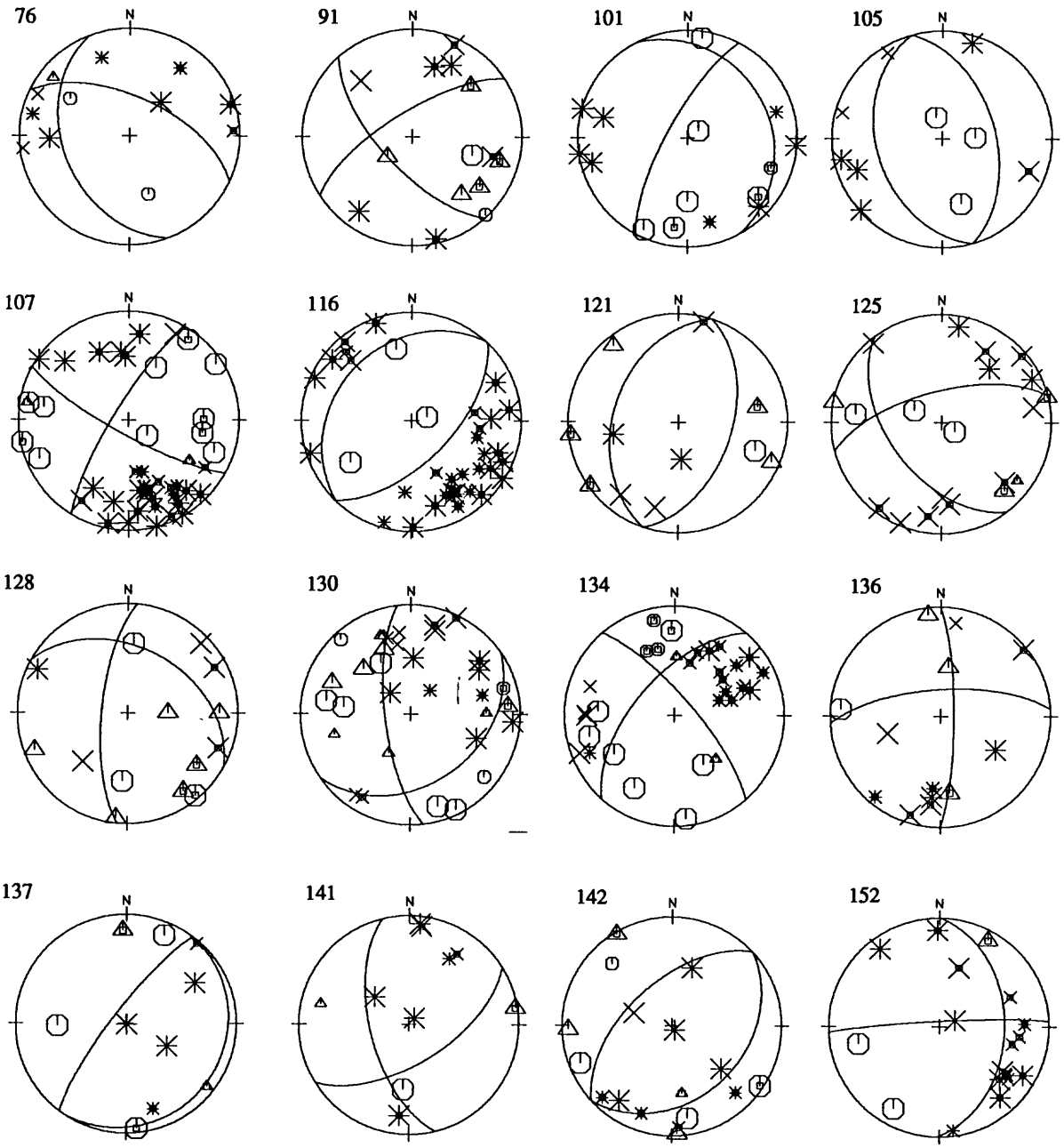

Figure A.3--Continued

Slab Earthquakes - cont.

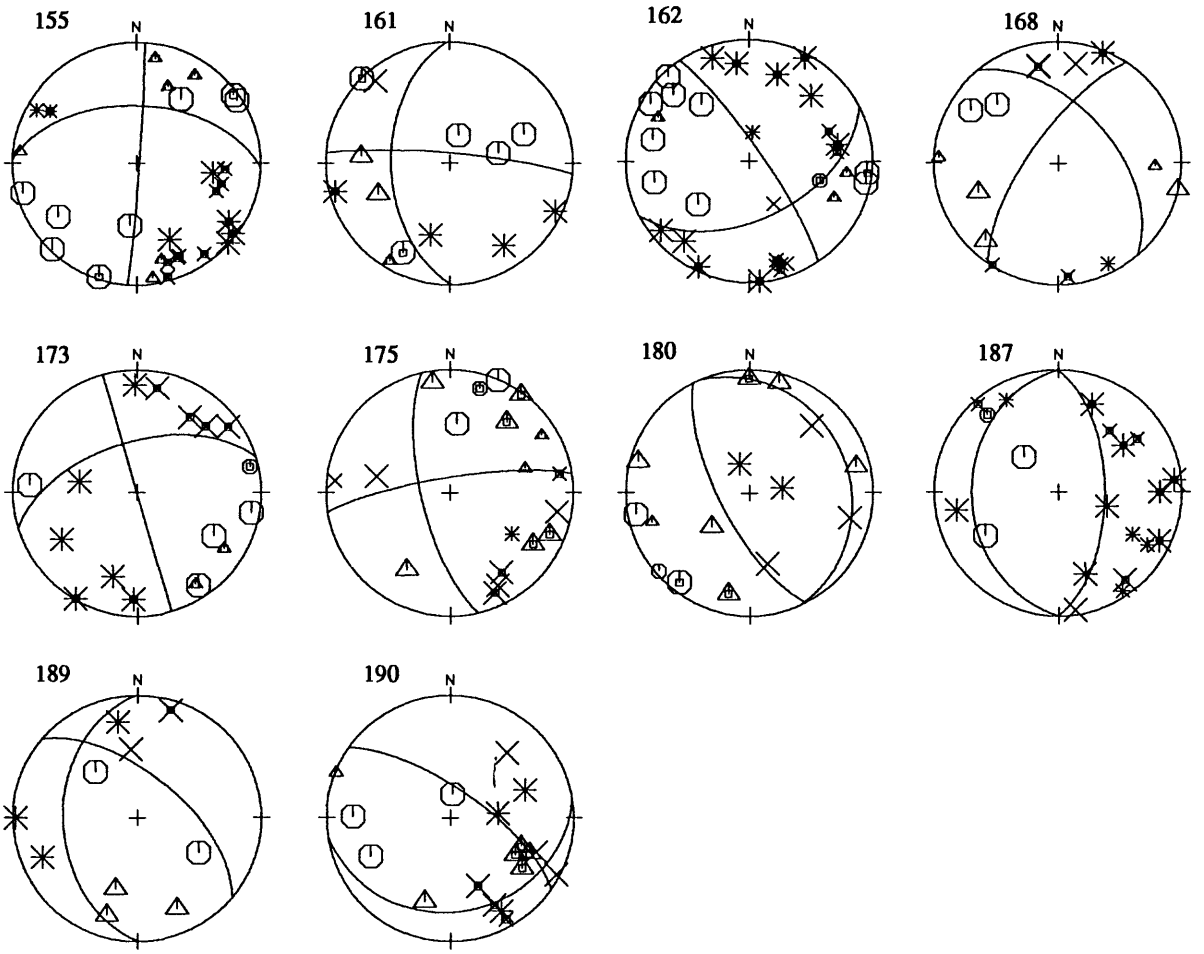

Figure A.3--Continued